Measurements of aerosol vertical profiles and optical properties during INDOEX 1999 using micro-pulse lidars

Running Title: Lidar measurements during INDOEX 1999
Submission to Journal of Geophysical Research - Atmospheres

Authors:

Ellsworth J. Welton [1], Kenneth J. Voss [2], Patricia K. Quinn [3],

Piotr J. Flatau [4], Krzysztof Markowicz [5], James R. Campbell [6],

James D. Spinhirne [7], Howard R. Gordon [2], and James E. Johnson [3]

1. GESTC, University of Maryland Baltimore County, Baltimore, MD 21250, USA
2. University of Miami, Physics Department, Coral Gables, Fl 33124, USA
3. Pacific Marine Environmental Laboratory, NOAA, Seattle, WA 98115, USA
4. Scripps Institution of Oceanography, UCSD, La Jolla, CA 92093, USA
5. Institute of Geophysics, University of Warsaw, 02093 Warsaw, Poland
6. Science Systems and Applications, Inc., Lanham, MD, 20706, USA
7. NASA Goddard Space Flight Center, Code 912, Greenbelt, MD 20771, USA

Corresponding Author Contact Information:

E. J. Welton
NASA-GSFC Code 912
Greenbelt, MD, 20771, USA
Ph: 301-614-6279
Fax: 301-614-5492
Email: welton@virl.gsfc.nasa.gov

Date: June 4, 2001

Abstract

Micro-pulse lidar systems (MPL) were used to measure aerosol properties during the Indian Ocean Experiment (INDOEX) 1999 field phase. Measurements were made from two platforms: the NOAA ship R/V Ronald H. Brown, and the Kaashidhoo Climate Observatory (KCO) in the Maldives. Sunphotometers were used to provide aerosol optical depths (AOD) needed to calibrate the MPL. This study focuses on the height distribution and optical properties (at 523 nm) of aerosols observed during the campaign. The height of the highest aerosols (top height) was calculated and found to be below 4 km for most of the cruise. The marine boundary layer (MBL) top was calculated and found to be less than 1 km. MPL results were combined with air mass trajectories, radiosonde profiles of temperature and humidity, and aerosol concentration and optical measurements. Humidity varied from approximately 80% near the surface to 50% near the top height during the entire cruise. The average value and standard deviation of aerosol optical parameters were determined for characteristic air mass regimes. Marine aerosols in the absence of any continental influence were found to have an AOD of 0.05 $\pm$ 0.03, an extinction-to-backscatter ratio (S-ratio) of 33 $\pm$ 6 sr, and peak extinction values around 0.05 km^{-1} (near the MBL top). The marine results are shown to be in agreement with previously measured and expected values. Polluted marine areas over the Indian Ocean, influenced by continental aerosols, had AOD values in excess of 0.2, S-ratios well above 40 sr, and peak extinction values approximately 0.20 km^{-1} (near the MBL top). The polluted marine results are shown to be similar to previously published values for continental aerosols. Comparisons between MPL derived extinction near the ship (75 m) and extinction calculated at ship-level using scattering measured by a nephelometer and absorption using a PSAP were conducted. The comparisons indicated that the MPL algorithm (using a constant S-ratio throughout the lower

troposphere) calculates extinction near the surface in agreement with the ship-level measurements only when the MBL aerosols are well mixed with aerosols above. Finally, a review of the MPL extinction profiles showed that the model of aerosol vertical extinction developed during an earlier INDOEX field campaign (at the Maldives) did not correctly describe the true vertical distribution over the greater Indian Ocean region. Using the average extinction profile and AOD obtained during marine conditions, a new model of aerosol vertical extinction was determined for marine atmospheres over the Indian Ocean. A new model of aerosol vertical extinction for polluted marine atmospheres was also developed using the average extinction profile and AOD obtained during marine conditions influenced by continental aerosols.

1. Introduction

Results from the 1996 pre-INDOEX cruise [*Krishnamurti et al.*, 1998] demonstrated that the Northern Indian Ocean is significantly affected by continental pollution during the winter monsoon season. Their analysis showed increases in the aerosol optical depth (AOD) over the ocean by as much as 0.2 and coincident reductions in the radiation reaching the surface. During the 1998 INDOEX field phase, more measurements of the aerosol distribution, optical properties, and resulting effects on the regional climate were made [*Rajeev et al.*, 2000]. The results showed significant clear sky aerosol radiative forcing over the Northern Indian Ocean [*Meywerk and Ramanathan*, 1999]. *Satheesh et al.* [1999] developed an aerosol model with a defined vertical structure for the tropical Indian Ocean using data from INDOEX 1998. Data was assimilated from lidar measurements in the Maldives and from several radiosonde launches to produce their vertical profile. Their vertical profile assumed that aerosol concentrations, and the relative humidity, were constant in the boundary layer, defined to be 1 km, and then decreased exponentially with altitude using a scale height of 800 m. The initial model calculations of AOD were found to be approximately 20% lower than in-situ measurements. The initial values were adjusted by incorporating a contribution from organic aerosols that were not actually measured at the surface, indicating that a complete understanding of the aerosol vertical structure is required.

Ansmann et al. [2000] have presented results from multi-wavelength Raman lidar measurements in the Maldives for a short period of time towards the end of INDOEX 1999. They found that a 3 km deep layer, advected from the Indian subcontinent, was situated over a polluted marine boundary layer. Furthermore, they report high values of both the AOD (~ 0.2 or higher) and the aerosol extinction-to-backscatter ratio (> 50 sr). Values such as these are typically only seen for continental aerosols in a polluted atmosphere. However, comprehensive

lidar measurements in terms of all day and night operation, and greater spatial coverage of both the southern and northern Indian Ocean are required to determine if the vertical distribution over the Maldives is indicative of the larger region. Recent advances in lidar technology now make it possible to perform lidar measurements continually (24 hours a day, 7 days a week) and from previously difficult field locations and platforms. Here we present measurements using a relatively new lidar system from a ship at sea. The deployment of the lidar on the ship allowed for more complete coverage over both the southern and northern Indian Ocean than was possible in earlier INDOEX field phases. The results, in conjunction with the earlier INDOEX measurements, provide data to scientists working on improving the models of aerosol vertical structure over the Indian Ocean [*Collins et al.*, 2000a; *Collins et al.*, 2000b].

Micro-pulse Lidar Systems (MPL) [*Spinhirne et al.*, 1995] were deployed during the 1999 Indian Ocean Experiment (INDOEX) field phase. A description of INDOEX is given by *Crutzen and Ramanathan* [this issue], and an overview of the results from INDOEX 1999 is given by *Coakley et al.* [this issue]. MPL systems were designed to operate semi-autonomously in the field and were the first eye-safe lidar systems capable of continuous operation. The MPL is small, rugged and easily adapted for installation on a variety of field platforms. During the experiment, an MPL was installed onboard the NOAA ship R/V Ronald H. Brown and another MPL was located at the Kaashidhoo Climate Observatory (KCO) in the Maldives. An overview of the R/V Ronald H. Brown measurements during INDOEX 1999 is given by *Dickerson et al.* [this issue]. An overview of the KCO measurement program is discussed by *Lobert et al.* [this issue].

MPL measurements were combined with sunphotometer AOD observations, data from radiosonde launches, and results from air mass back-trajectories to answer questions that arose

from earlier INDOEX findings, and to judge whether aerosol profiles over the Maldives are indicative of the larger region. Measurements of aerosol layer heights were made to determine if the vertical structure used in earlier models is sufficient to use for all locations in the region and for a variety of air mass transport patterns. Measurements of aerosol layer optical properties, such as the AOD (including night-time measurements using the MPL), were made to determine if there is a noticeable dependence on geographic region and air mass transport. In particular, joint measurements of aerosol layer height, AOD, humidity profiles, geographic location, and air mass back-trajectories over a several week period were sought to provide a valuable database for future modeling efforts. Finally, determination of the variability of the aerosol extinction-to-backscatter ratio over the Indian Ocean was sought to improve lookup tables of this parameter that are needed for algorithms to be used by satellite lidar projects such as the Geoscience Laser Altimeter System (GLAS) [*Palm et al.*, 2001]. Further information on INDOEX MPL measurements and access to data described here is available at the NASA-GSFC MPL-Net web-site (http://virl.gsfc.nasa.gov/mpl-net/).

2. Instrumentation

2.1 Micro-pulse Lidar System

Vertical measurements of aerosols and clouds were made using a micro-pulse lidar system (MPL) [*Spinhirne et al.*, 1995]. The MPL was developed at NASA-GSFC and is now commercially manufactured by Science & Engineering Services Inc., Burtonsville, MD, USA. The MPL is a compact and eye-safe lidar system capable of determining the range of aerosols and clouds by firing a short pulse of laser light (at 523 nm) and measuring the time-of-flight from pulse transmission to reception of a returned signal. The returned signal is a function of time, converted into range using the speed of light, and is proportional to the amount of light

backscattered by atmospheric molecules (Rayleigh scattering), aerosols, and clouds. The MPL achieves ANSI eye-safe standards by using low output energies (μJ), and beam expansion to 20.32 cm in diameter. The MPL laser pulse duration is 10 ns with a pulse-repetition-frequency of 2500 Hz and output energies in the μJ range. The high PRF allows the system to average many low energy pulses in a short time to achieve a good signal-to-noise ratio.

Raw data acquired by the MPL are stored in daily-concatenated binary files. The MPL signals are averaged and stored at 1-minute time intervals, with a range resolution of 0.075 km from sea level up to a maximum altitude of 30 km. The raw signals include effects caused by features of the MPL design. The most important effects include noise induced in the detector by the firing of the laser, and overlap (which determines the nearest range at which the MPL can accurately image returned signals). Raw MPL signals are corrected for these instrumental effects using procedures discussed in Appendix A.

2.2 Ship

An MPL was deployed onboard the NOAA ship R/V Ronald H. Brown during the INDOEX 1999 IFP. Figure 1 displays the ship track during Leg 1 and Leg 2 of the cruise. The day of year (DOY) is given for each day along the track. The leg 1 cruise started from the island of Mauritius in the southern Indian Ocean (day 53). The ship then sailed northeast, crossing the equator on day 58, and arrived at Male, Maldives on day 59 at the conclusion of leg 1. Leg 2 began on day 63 as the ship sailed from Male to a fixed point just off of the KCO site. The ship performed an intercomparison with KCO from day 63.75 to 64.75. The ship then sailed north to the Arabian Sea, and performed an intercomparison with the R/V Sagar Kanya from day 68.5 to 69.5. The ship reached its most northern point on day 70. The ship then headed south, and on day

72, turned east and headed to the vicinity of the Maldives islands. The results presented here include data taken up to day 75 of leg 2.

The MPL was installed inside a climate controlled housing, forward of the ship's smokestack, and operated continuously except during mid-day. The MPL was turned off approximately +/- 1 hour of solar noon to prevent direct sunlight from entering the MPL receiver and damaging the detector. Measurements were made throughout the cruise to acquire data needed to correct the raw signals for instrument effects including afterpulse and overlap (Appendix A). Afterpulse measurements were made throughout the cruise by simply covering the system periodically and measuring the afterpulse noise. A successful overlap measurement was performed on the ship during a period of clear air and very calm seas in the SH doldrums (near the start of the cruise). After the corrections were applied, the MPL data products were calculated. The MPL data products and processing routine are described in Appendix A.

Microtops Sunphotometer

A Microtops sunphotometer (Solar Light Co.) was operated several times each day to acquire measurements of the AOD (380, 440, 500, 675, and 870 nm). Voss et al. [2001] report that the AOD error for this instrument was ± 0.01 during the Aerosols99 cruise immediately prior to the start of INDOEX (time between the Aerosols99 and INDOEX cruises was ~3 days). The AOD at the MPL wavelength (523 nm) was determined by fitting the data to a power law [*Angstrom*, 1964]. The Microtops AOD at 523 nm were used only to calibrate the MPL during the cruise, and the sunphotometer AOD error of ± 0.01 was used in the determination of the MPL calibration (Appendix A).

Radiosondes and Back-trajectories

Radiosondes were launched by the ship's crew three times each day (at approximately 0000, 1200, and 1800 UTC). Radiosonde data was used to determine temperature and humidity profiles during the cruise. Hysplit back-trajectories [*Draxler and Hess*, 1997] were processed for each day during the cruise [*Dickerson et al.*, this issue]. Seven day back-trajectories with end points at 0.5, 2.5, and 5.5 km were performed at 6-hour intervals each day of the cruise.

Nephelometer and Particle Soot Absorption Photometer

Measurements of aerosol scattering and absorption on the ship (19 m) were made using an integrating nephelometer (TSI model 3563, 550 nm) and a particle soot absorption photometer (PSAP, Radiance Research, 565 nm). The scattering and absorption measurements were conducted at 55% relative humidity. The scattering values were adjusted to ambient humidity using functions determined during ACE-1 [*Carrico et al.*, 1998] for marine conditions, and functions determined at KCO [*Andrews et al.*, this issue] for continental conditions. The absorption values were assumed to be independent of humidity. Extinction at the ship was calculated by adding the humidity-adjusted scattering values to the absorption.

2.3 KCO

An MPL was installed at KCO during the INDOEX 1999 IFP. KCO is located in the Maldives at 4° 58′ N and 73° 28′ E and its location with respect to the ship track is apparent in Figure 1. The MPL operated continuously from day 41 to 86. The MPL was installed inside a climate-controlled housing, and was fixed at a zenith angle of 33 degrees to avoid direct sunlight close to solar noon. Measurements were also made at KCO to correct the raw signals for afterpulse and overlap effects. A successful afterpulse measurement was made by simply covering the system and measuring the afterpulse noise.

A successful overlap correction at KCO was not possible. The maximum elevation at KCO was not sufficient to raise the MPL far enough above the turbulent atmosphere near the ocean's surface, as a result breaking waves along the island's atoll created conditions of horizontal in-homogeneity during the overlap measurements. Also, the relatively high and constant levels of pollution at KCO made for increased difficulty in finding periods of horizontal homogeneity in the aerosol plumes. More frequent overlap measurements may have resulted in finding some conditions of homogeneity during periods of low surface winds and clear air, but this was not possible due to lack of a full-time on-site MPL operator at KCO. As a result, the near range structure (< 3 km) of the MPL signals could not be determined for the KCO data set.

AERONET Sunphotometer

An AERONET sunphotometer [*Holben et al.*, 1998] was installed at KCO during 1998, and continued operation through the 1999 IFP. The AERONET AOD (380, 440, 500, 670, and 870 nm) was used to determine the AOD at the MPL wavelength (523 nm) by fitting the data to the Angstrom power law. The AERONET AOD at 523 nm was used to calibrate the KCO MPL in the same manner as done on the ship. AERONET reports AOD error bars ± 0.01 in magnitude, and these were used to determine the KCO MPL calibration error (Appendix A).

3. Results

The raw MPL data from both the ship and KCO were corrected for instrument effects and data products were processed using an algorithm developed to process large sets of MPL data. A summary of the data products and error estimates is given here. A complete description of the products is given in Appendix A, along with an overview of the algorithm.

The first step in the data processing routine is the calibration of the MPL. During INDOEX the calibration zone (Appendix A) was set between 6 and 7 km after inspection of the

signals indicated that no significant aerosols were present at that altitude. Each MPL was then calibrated using the AOD from the sunphotometer measurements on the respective platform. Periodic calibrations were made during cloud-free periods of the experiment and a linear interpolation was used to generate calibration values for any time during the experiment. The error of the lidar calibration constant was $\pm$ 5% for both MPL systems.

After calibration was performed, the following data products were calculated: the top of the MBL, the height of the highest aerosols detected (top height), AOD, aerosol extinction profiles (from the surface to the top height), and the average aerosol extinction-to-backscatter ratio (S-ratio) from the surface to the top height. As mentioned in the Appendix, the measured AOD is the optical depth from the surface to the top height and is obtained independently of the aerosol layer parameters (such as the S-ratio) by determining the transmission loss from the surface to the top height. The extinction profile and S-ratio are both determined using the measured AOD and an assumption of constant S-ratio from the surface to the top height. The implications of this choice are discussed in more detail later on.

The estimated baseline error for the AOD was $\pm$ 0.02 for the MPL systems, and the baseline error in determining aerosol layer heights is estimated at $\pm$ 0.075 km. The baseline error for extinction values in a profile is estimated to be $\pm$ 0.005 km^{-1}, and $\pm$ 5 sr for the S-ratio. Actual error bars on individual measurements may be larger than the baseline errors due to signal noise. Error bars for the data products are dependent upon atmospheric conditions and background sunlight levels (lower error bars at night). The data given below all include actual error bars calculated using the baseline error values and a determination of the signal noise during that measurement.

3.1 MPL Data

Aerosol extinction profiles from Legs 1 and 2 are displayed in Figure 2 and Figure 3, respectively. The corresponding MBL top, aerosol top height, AOD, and S-ratio values for the 30 minute cloud screened averages are shown as a function of DOY in Figures 4a, 4b, and 4c respectively. The gap in data from day 60 to 63 is the period between Leg 1 and Leg 2 when the ship was in port at Male. Smaller gaps in the data exist and are mostly due either to periods when the MPL was turned off near solar noon, or to periods when the data products could not be determined with any certainty because of large error bars (~ 100% error or more). The latter cases were caused primarily by very low signal-to-noise due to a combination of mid-day sunlight and high AOD (increased attenuation through the layer). A few of the 30 minute time averaged periods contained clouds throughout and it was not possible to analyze them, however, this was not frequent.

The same parameters are plotted versus the ship latitude in Figures 5a, 5b, and 5c to show latitudinal variations in the aerosols during the cruise. The S-ratios displayed in Figure 5c do not show a strong trend with latitude, but this is not so with the other data. In general, the Northern Hemisphere (NH) AOD values were at least double the values found in the Southern Hemisphere (SH). For most of the SH, only the aerosol top height was found using the algorithm presented in Appendix A, and the MBL top could not be determined. Both the aerosol top height and the MBL top were determined for most of the NH. Latitudinal variations in the data are discussed further in section 4, and are shown to be due to changes in air mass characteristics.

MPL Data from KCO

A limited data set was produced for the KCO MPL due to lack of an accurate overlap correction (Appendix A). This problem did not affect the measurement of the top height or the

AOD because they are not dependent on the overlap correction as long as the overlap range is below the top height. The overlap range of the KCO MPL was below 3 km (and below top heights in the NH) because the system was aligned in the near field, which decreased the overlap range below normal (typically above 4 km for normally aligned systems). Current MPL systems are normally aligned to the far field so they can correctly determine both boundary layer properties (after overlap correction) and high level cloud properties (such as cirrus optical depths). This study focuses only on the boundary layer, and therefore the KCO MPL data can be used to determine the top height and the AOD. However, determination of the MBL top, the extinction profile, and the S-ratio were not possible because they are dependent on the overlap correction.

Figure 6a and 6b show the top height and the AOD, respectively, measured by the KCO MPL. The top height at KCO was between 3 and 4 km for the majority of the experiment, in agreement with top height measurements on the ship in the NH. Maximum AOD values at KCO ranged from about 0.5 to 0.7 in value. Therefore, the KCO AOD was comparable to the ship MPL AOD values in the NH, although the KCO AOD tended to reach higher maximum values.

The ship performed an inter-comparison with KCO and the MBL tops, top heights, and AOD were compared between the two platforms. Figure 7a and 7b show the results of this comparison. Individual error bars were omitted from the plots to produce a clear presentation of the results. Figure 7a shows that the top heights from the ship MPL and the KCO MPL agree within 100 m (approximately equal to the average error bar for the heights during this comparison). Figure 7b shows the AOD comparison between the ship MPL and the KCO MPL. The AOD from the ship microtops and the KCO AERONET sunphotometer are also shown for comparison. The ship microtops and ship MPL AOD values are not independent of each other

because the microtops was used to calibrate the ship MPL. The same relationship exists between the KCO AERONET sunphotometer and KCO MPL AOD values. However, comparisons between ship derived AOD and KCO derived AOD values do represent an independent comparison. On average, the AOD agree better than $\pm$ 0.05 (approximately equal to error bars for the MPL derived AOD during this comparison).

3.2 Grouping of MPL and Radiosonde Data by Air Mass Trajectory

The ship results discussed in the previous section were clustered together into separate categories defined by consecutive days with similar, characteristic air mass trajectories. Table 1 defines the categories (C1 to C6) and shows the air mass origin for each trajectory altitude level in the category. The air mass origins defined by *Dickerson et al.* [this issue] are used in Table 1 to describe the origin of each trajectory. *Dickerson et al.* define categories in their paper using these descriptions. However, they focus only on the 0.5 km trajectory, therefore their categories are grouped differently than ours. The categories presented here also include the 2.5 km and 5.5 km trajectory. As shown below, only the C2 data had a top height above 4 km and therefore the 5.5 km trajectory was considered only important for C2.

Category C1 only occurred in the SH and was characterized by air mass trajectories at all altitudes that originated over the middle of the Southern Indian Ocean. Category C2 only occurred in the SH, and was characterized by air mass trajectories at 0.5 and 2.5 km from over the SH, but the air mass at 5.5 km that actually originated near the surface over the Northern Indian Ocean (at approximately 10° N). Category C3 only occurred near the equator, and was characterized by air masses at 0.5 km that originated far to north (at $\simeq$ 10° N). C3 air masses at 2.5 km originated over the SH. Category C5 occurred only in the NH off the western coast of India, and was characterized by air masses at 0.5 km that originated over north-western India and

Pakistan, and moved south over the ocean until arriving at the ship. C5 air masses at 2.5 km originated over the southern portion of India and traveled a short distance to the ship. The C6 category occurred at the northern-most portion of the cruise (in the Arabian Sea), and was characterized by 0.5 km air masses that originated over Iran, and moved south-east over the ocean, until arriving at the ship. C6 air masses at 2.5 km originated over southern Saudi Arabia and Yemen, and moved east until arriving at the ship.

Air mass types that did not fit into one of those listed above were grouped together into the C4 category. The C4 category occurred in the NH and contained the most abundant air mass types encountered during the cruise. Three distinct air mass trajectories were grouped together to form the C4 category. Pattern one was characterized by a 0.5 km air mass that originated over the southern tip of India, and a 2.5 km air mass that came from the south but originated over the ocean in the NH. Pattern two was characterized by air masses at all altitudes that both originated over the southern tip of India. Finally, pattern three was characterized by a 0.5 km air mass that originated over north-western India and Pakistan, and a 2.5 km air mass that came from the south but originated over the ocean in the NH.

Figures 8a and 8b display the characteristic trajectories for each category. Figures 9a, 9b, and 9c show the average extinction, humidity, and temperature profile for each category. The temperature and humidity profiles were generated using data from the radiosonde launches in that category. The standard deviation for the average profiles is indicated by the bars on each graph. No radiosondes were launched during the C2 time period, and only one was launched during C3, therefore no temperature and humidity profiles are shown for these categories. Figures 10a, 10b, and 10c show the average MBL top, aerosol top heights, AOD, and S-ratio for each category with bars representing the standard deviation in the values.

Figure 11 shows comparisons between the C1, C4, C5, and C6 S-ratios measured on the ship, and S-ratios that have previously been published. The C2 and C3 categories did not have sufficient radiosonde launches to accurately determine the humidity range and their S-ratio values are not shown on the plot. The previously published S-ratio values, shown in Figure 11, include theoretical calculations conducted by *Ackermann* [1998] for marine, continental, and desert aerosols as a function of humidity, island based measurements of saharan dust [*Welton et al.*, 2000], ship measurements in marine and smoke (biomass) environments [*Voss et al.*, 2001], and island based Raman lidar measurements in the Maldives during INDOEX [*Ansmann* et al., 2000]. *Doherty et al.* [1999] also determined the S-ratio in-situ using measurements of extinction (nephelometer and PSAP) and measurements of backscatter from a 180° backscatter nephelometer. Their results are not displayed in Figure 11 because they do not report a specific value of humidity. However, they show that for humidity less than 40% continental aerosols had an S-ratio between 60 and 70 sr, and marine aerosols had an S-ratio of approximately 20 sr, all with uncertainties on the order of 20%.

The Raman lidar technique allows the S-ratio to be calculated at each altitude bin (down to a minimum height) rather than as a layer averaged value, therefore the S-ratios from *Ansmann et al.* are shown segmented according to height (above and below 1.5 km). Also, the modeled desert S-ratio by *Ackermann* was done using Mie theory and could have large errors due to the assumption of particle sphericity, but is shown here for a comparison of what typical models would assume for desert and dust-like aerosols. In fact, based upon findings given in *Mishchenko et al.* [1997], when using Mie theory to calculate dust S-ratios one would expect to get a lower value compared to using a more realistic particle shape. This is because the dust phase function at 180° is overestimated using Mie theory, and the S-ratio is inversely proportional to the phase

function (Appendix A). This effect is demonstrated in Figure 11. The saharan dust S-ratio by *Welton et al.* was measured independent of particle shape, and is almost twice the value of the *Ackermann* model.

4. Discussion

This section discusses comparisons between MPL derived extinction near the surface, with extinction determined at ship-level. The results from each air mass category are then discussed in detail. The findings are then used to determine if the model for vertical aerosol extinction is applicable to the greater Indian Ocean region.

4.1 Extinction Comparisons Near the Surface

Quinn et al. [this issue] report measurements of aerosol scattering and absorption at the ship (19 m) using the nephelometer and PSAP discussed in section 2. Extinction at the ship was calculated by combining the two measurements after adjusting the scattering values to ambient humidity. The ship-level extinction data was then segmented into the same categories given in Table 1. The ship-level extinction values for each category were compared to the corresponding MPL extinction values at 75 m (the lowest altitude bin in the MPL data). A similar study was conducted during the Aerosols99 cruise across the Atlantic [*Voss et al.*, 2001].

Figure 12 shows the ship-level extinction plotted versus the MPL extinction at 75 m, and the 1:1 line is given for reference. The C1, C3, and C4 MPL extinction values slightly overestimate extinction compared to the ship-level values, but the agreement is better than for the C2, C5, and C6 categories. MPL derived near-surface extinction values from the latter categories do not agree well with extinction at ship-level and significantly overestimate extinction near the surface.

The primary reason for this comparison was to gauge the overall applicability of using a constant S-ratio for the INDOEX data. In order to do this, we must first obtain an indication of the magnitude of vertical mixing between the MBL and the aerosols above. An in depth discussion of entrainment between a boundary layer and a layer situated directly on top has been published by *Russell et al.* [1998]. They show that bi-directional mixing between the layers can occur and is dependent upon the amount of turbulence at the layer interface. As a gross measure of turbulence, we use the intensity of the MBL inversion. We then make the simple assumption that periods with a fairly weak inversion will have some degree of bi-directional mixing, and those with a strong inversion will not. This simple model was used to roughly assess the usefulness of a constant S-ratio during INDOEX.

Figure 9c shows that a strong temperature inversion was present at the top of the MBL during C5 and C6. There is also a marked change in the humidity profile just above the MBL. Using our simple model, these conditions indicate that the MBL for C5 and C6 was not well mixed with the aerosols above. However, there was not a strong temperature inversion for the C1 and C4 categories. This indicates that aerosols in the MBL and above were mixed together in the C1, C3, and C4 regions. This determination was not conducted for C2 and C3 because of the lack of radiosonde data.

Our data processing routine (Appendix A) assumes that within a given aerosol layer, the S-ratio is constant with altitude and uses the AOD (obtained in a prior step) to constrain the calculation of the extinction profile throughout the layer. Simulations show that when the true S-ratio in a layer is relatively constant (roughly $\pm$ 15%), then the algorithm will reproduce an average S-ratio and extinction profile with an error percentage nearly equal to the percent fluctuation in the true S-ratio [unpublished results]. If two layers are present, but there is not at

least 1 km of clean air between them, then the algorithm can not distinguish the two layers and they must be treated as one for the calculation of AOD, S-ratio, and extinction. In such a case, if the real S-ratios between the two layers are different, then the algorithm will calculate an S-ratio that is an average of the two real layer S-ratios [*Welton*, 1998]. This means that if the real S-ratio in layer 1 is lower than the real S-ratio in layer 2, the extinction calculated in layer 1 will be overestimated because it is proportional to the average S-ratio. Likewise, the extinction in layer 2 will be underestimated.

The previous discussion assumes that the S-ratio was dependent only upon aerosol type, and therefore as long as the aerosols in a layer are the same type the S-ratio is constant in that layer. However, changes in humidity throughout both the MBL and above are evident in Figure 9b. This could cause changes in the S-ratio throughout each layer even if there was only one aerosol type present. Figure 11 presents the humidity dependence of the S-ratios modeled by *Ackermann*. The marine S-ratio varies by only ~ 10 sr from 0 to 100% humidity. The continental S-ratio varies by the same amount for the humidity ranges observed during INDOEX. This indicates that there should only be small changes in the S-ratio (< 10 sr) due to humidity changes with altitude. Therefore, we assume that the altitude dependence of the S-ratio is only due to changes in the type of aerosols between layers.

The effects discussed above are possible causes for the agreements and disagreements in near surface extinction comparisons between the MPL and the ship. Namely, that the C1 and C4 categories had a MBL that was well mixed with the aerosols in the layer above, but the C5 and C6 categories contained a MBL that was not well mixed with aerosols above and therefore contained two distinct aerosol layers. In the first situation, a constant S-ratio is reasonable and the extinction profile should be fairly correct. The latter situation implies that the most likely

scenario would be for the MBL to have a marine-like S-ratio (~ 30 sr or lower), and the aerosols above would be of continental origin with an S-ratio of ~ 55 sr or higher. Since the algorithm has to analyze the two layers as one, it would calculate an average S-ratio somewhere between the two and also overestimate extinction near the surface because the higher average S-ratio was used in the MBL. While there was no radiosonde data for C2, a weak aerosol layer above 4 km was detected which means that the aerosols above were probably not well mixed with the MBL. This is a possible cause of the significant overestimation of ship-level extinction by the MPL. The implications of these findings are further explored when discussing the results from each category.

It is worth noting that other errors could factor into the comparisons shown in Figure 12. The MPL near surface signals have to be corrected for overlap effects and if the correction is not accurate then the signals closest to the surface will suffer the most. However, gross error in the overlap correction would manifest as a systematic and constant offset in the MPL signal values near the surface. This was not observed during the cruise. Another possible source of error could lie in the functions used to adjust the ship scattering values to ambient humidity and could possibly lead to substantial errors in the ship-level extinction values. Despite this potential problem, we present this method as the best option to assess the usefulness of using a constant S-ratio for lidar studies because the two forms of measurement were co-located and acquired data together non-stop during the cruise. As more is learned about the hydroscopic properties of different aerosol types, this method will improve as an independent determination of lidar results.

4.2 Summary of the Results From Each Category

The MPL derived results from each category are listed in Table 2. The humidity varied from ~ 80% near the surface to ~ 50% at the top height for each category. As shown below, only the C1 category is representative of a marine atmosphere, while all the others have been influenced by continental aerosols to varying degrees. This section discusses the findings from each category in more detail.

C1

Quinn et al. [this issue] report that sea-salt dominated the surface chemistry measurements. The aerosol extinction at the surface was 0.03 km^{-1} and increased slightly to a peak value of 0.04 km^{-1} near the top of the MBL, then decreased to the top height. The C1 AOD was characteristic of clean marine environments we have previously encountered [*Welton*, 1998; *Voss et al.*, 2001]. The S-ratio value for this region compares well with the other marine S-ratios displayed in Figure 11. The results from section 4.1 indicate that the aerosols well mixed between the MBL and above, and therefore the S-ratio and extinction profile obtained for C1 should not have been greatly affected by the assumption of a constant S-ratio (used in the algorithm). This is supported by the fact that the MPL derived near-surface extinction was similar to the ship-level extinction in Figure 12. From the results given above, the atmosphere in the C1 region is termed characteristic of a marine environment.

C2 and C3

Quinn et al. [this issue] report that sea-salt dominated the surface chemistry measurements. The aerosol extinction at the surface was 0.04 km^{-1} and increased to a peak value of 0.09 km^{-1} near the top of the MBL, then decreased until reaching an altitude of ~ 3 km. The extinction then began to increase slightly and a weak aerosol layer was detected up to the top

height, and had extinction values on the order of 3.5E-3 km^{-1}. The C2 AOD was also characteristic of clean marine environments we have previously encountered [*Welton*, 1998; *Voss et al.*, 2001]. However, the S-ratio did not agree with the other marine S-ratios displayed in Figure 11, and instead is more similar to a continental value. The MPL derived near-surface extinction was significantly greater than the ship-level extinction in Figure 12. It is likely that the high altitude aerosols were continentally influenced because they came from a region in the NH where high AOD was later measured, and the aerosols below were marine in nature due to their source region over the southern Indian Ocean. The high altitude aerosols did appear to influence the calculation of the S-ratio and the extinction values for the C2 region.

Quinn et al. [this issue] report that sea-salt dominated the surface chemistry measurements. The aerosol extinction at the surface was 0.03 km^{-1} and increased slightly to a peak value of 0.05 km^{-1} near the top of the MBL, then decreased to the top height. The C3 AOD was characteristic of clean marine environments we have previously encountered. However, the S-ratio did also not agree with the other marine S-ratios displayed in Figure 11. The MPL derived near-surface extinction was similar to the ship-level extinction in Figure 12, and it is possible that the aerosols were well mixed between the layers. The high S-ratio value obtained for C3 indicates that continental aerosols were transported from the NH to the C3 region (near the equator).

For these reasons, C2 and C3 are not considered typical marine atmospheres despite the fact that their regions were far from land. Instead, the atmospheres in C2 and C3 have been influenced by continental sources.

C4

The C4 region was in the NH and was characterized by one of three main air mass trajectories: long range transport over northern Indian Ocean at all altitudes, short range transport from India at all altitude levels, or short range transport from India at the surface, but from over the northern Indian Ocean at mid-level altitudes. *Quinn et al.* [this issue] show that the C4 surface concentrations of sub-micron nss-Sulfate and potassium increased dramatically compared to the C1, C 2, and C3 categories. The nss-Sulfate and potassium reached the highest concentrations in C4, compared to all other categories. Sea-salt concentrations at the surface did not change significantly compared to levels in C1, C2, and C3.

The aerosol extinction at the surface was 0.14 km^{-1} and increased to a peak value of 0.20 km^{-1} near the top of the MBL, then decreased to the top height. The C4 AOD was similar to values previously measured over the ocean during periods of continental influence [*Voss et al.*, 2001]. The S-ratio value for this region compares well with the modeled continental S-ratio displayed in Figure 11, and also with S-ratios measured during periods of continental influence [*Voss et al.*, 2001]. The S-ratio is much lower than the value reported by *Ansmann et al.* [2000], which also describes an otherwise marine environment (the Maldives) that has been influenced by continental sources. The results from section 4.1 indicate that the aerosols should be well mixed between the MBL and above, and therefore the S-ratio and extinction profile obtained for C4 should not be greatly affected by the assumption of a constant S-ratio. This is also supported by the fact that the MPL derived near-surface extinction was similar to the ship-level extinction in Figure 12.

The difference between the C4 S-ratio and the value reported by *Ansmann et al.* could be due to differences in the aerosols between the measurement periods (*Ansmann et al.* report a

single value measured at the end of March). It could also be due to our assumption of a constant S-ratio. The latter implication calls for more study regarding the usefulness of constant S-ratios in lidar studies. However, to truly gauge whether the S-ratios over the Maldives are routinely as high as reported by *Ansmann et al.*, requires that more Raman lidar S-ratios be reported than just the single measurement period. Despite differences between the C4 S-ratio value and the *Ansmann et al.* value, it is clear that they are much higher than a typical marine atmosphere could produce. Therefore, the C4 region also has an atmosphere that has been influenced by continental sources.

C5

The C5 region was in the NH and was characterized by surface level air masses that originated over north-western India and Pakistan, and moved south over the ocean for several days until arriving at the ship. The 2.5 km air mass originated over the southern tip of India and transported a short distance to the ship's location. *Quinn et al.* [this issue] show that the C5 surface concentrations of sub-micron nss-Sulfate and potassium decreased significantly compared to levels in the C4 category, although the concentrations were still higher than levels in C1, C2, and C3. Conversely, the C5 sea-salt concentrations at the surface increased considerably compared to levels in C4, and were even larger than concentrations in C1 (dominated by sea-salt).

The aerosol extinction at the surface was 0.13 km^{-1} and increased to a peak value of 0.19 km^{-1} near the top of the MBL. The extinction then decreased until it reached a minimum of 0.07 km^{-1} at an altitude of 1.5 km. The extinction then began to increase again to a peak value of 0.11 km^{-1} at an altitude of 2.4 km, before finally decreasing until reaching the top height. The C5 AOD was also similar to values previously measured over the ocean during periods of

continental influence [*Voss et al.*, 2001]. Figure 11 shows that the C5 S-ratio value is higher than other marine values, but also lower than both the modeled continental S-ratio and the S-ratios measured during periods of continental influence. However, the standard deviations of the C5 S-ratio and the continental and marine values do show that there is quite a bit overlap between them (*Ansmann et al.* values excluded).

The results from section 4.1 show that the MBL was not well mixed with the aerosols above. The surface concentration measurements show that the MBL was more marine-like then during C4 conditions, possibly due to the long transport time of the air mass over the ocean. Also, the air mass at 2.5 km originated over India (continental) and was only a day or two old. Therefore, with a continental layer over a more marine-like layer, the MPL derived near-surface extinction should be significantly greater than the ship-level extinction (as was found). Also, the algorithm should, and did, calculate an S-ratio that is between values expected for marine and continental aerosols.

C6

The C6 region was in the Arabian Sea and was characterized by surface air masses that originated over Iran, and moved south-east over the ocean, until arriving at the ship. The 2.5 km air masses originated over southern Saudi Arabia and Yemen, and moved east until arriving at the ship. *Quinn et al.* [this issue] show that the C6 surface concentrations of sub-micron nss-Sulfate and potassium were lower than levels in both C4 and C5, although the concentrations were slightly higher than levels in C1, C2, and C3. However, the C6 sea-salt concentrations at the surface were quite high and comparable to the concentrations in C1 (dominated by sea-salt). Residual mass concentrations, thought to be dust, were found to be quite large.

The aerosol extinction at the surface was 0.09 km^{-1} and increased to a peak value of 0.14 km^{-1} near the top of the MBL. The extinction then decreased until it reached a minimum of 0.02 km^{-1} at an altitude of 1.2 km. The extinction then began to increase again to a peak value of 0.05 km^{-1} at an altitude of 2.4 km, before finally decreasing until reaching the top height. Figure 11 shows that the C6 S-ratio value is also higher than marine values, but comparable to both the modeled continental S-ratio and also the S-ratios measured during periods of continental influence. The S-ratio was higher than both the modeled desert and measured dust values.

The results from section 4.1 indicate that the MBL was not well mixed with the aerosols above. The surface concentration measurements show that the MBL contained less pollution aerosols and more sea-salt then were found in the highly polluted C4 region. The concentration data also showed the possible presence of dust. The air masses at all altitudes originated over land, and from regions were dust is expected, and also spent approximately the same time over the ocean before reaching the ship. However, the aerosols above the MBL should not contain significant sea-salt and in that regard are not similar to the aerosols in the MBL.

For these reasons, the MPL derived near-surface extinction will not agree well with the ship-level extinction values, and this was in fact determined to be true (Figure 12). Therefore, the presence of a distinct aerosol layer over the MBL did influence the calculation of the S-ratio and the extinction over the Arabian Sea.

Comparison of Vertical Aerosol Extinction: Model vs. Measured

The results presented above show that using our algorithm (constant S-ratio), correct extinction values are only expected for the C1 and C4 categories. The overall magnitudes of the extinction values in the C2, C5, and C6 categories may be incorrect due to assumptions of constant S-ratio in our algorithm. No determination was possible for C3.

However, the shape of the extinction profile, in other words the locations of peaks and minimums, is not as affected by this problem. This is because the backscatter profile is actually calculated from the MPL signals, not extinction (see Appendix A). The extinction profile is obtained afterwards by multiplying the calculated backscatter by the S-ratio. The calculated backscatter profiles are not as dependent upon the use of a constant S-ratio because the MPL measures signals that are directly proportional to backscatter. Extinction is only present in the transmission term of the lidar signal, and is therefore a weaker component than backscatter. For this reason, minimums and peaks within a profile are fairly accurate depictions of the overall shape of the aerosol's vertical distribution. This is verified by comparing the shape of the measured lidar signal profile to that of the calculated extinction. The overall shape of both profiles were the same for every category. Therefore, the extinction profiles measured in all the categories can be used to assess how well a model might determine the overall shape of the aerosol's vertical distribution. However, to compare the actual measured extinction magnitudes from the MPL to those from a model or other instruments, one should only use results from the C1 and C4 categories.

Figure 9a shows that, for all categories, the shape of measured MPL profiles did not agree with the profile proposed by *Satheesh et al.* [1999]. In every category, extinction below 1 km was not constant as in the model. Extinction was found to increase from the surface up to a peak value just below the top of the MBL, which was below 1 km throughout the cruise. This increase in extinction throughout the MBL is similar to that proposed by *Fitzgerald* [1989]. Disagreements also existed for altitudes above the MBL. The C1, C3, and C4 categories did show that the extinction decreased with altitude above 1 km, but that the extinction did not reach zero by a scale height of 800 m (above 1 km) as proposed by the model. Also, the C2 category

showed the presence of a weak aerosol layer far above the proposed scale height layer top. Figure 9a also shows that the C5 and C6 categories have a profile shape above 1 km that is significantly different than the *Satheesh et al.* model. The C5 and C6 extinction profiles show that the extinction did not decrease exponentially above 1 km as the model proposed, but rather that the extinction increased to a peak at 2.4 km and then fell off with altitude (reaching zero below 4 km).

The C1 and C4 extinction profiles had a similar shape, and together they were the dominant air mass conditions during the cruise. A characteristic extinction profile that represents most conditions over the Indian Ocean region would be best represented using the results from these categories. The C1 results were used to build a new model of extinction over the Indian Ocean for the SH and clean pollution-free air masses over the NH. The C4 results were used to build a new model of extinction for polluted air masses over the Indian Ocean in the NH. The models are termed marine and polluted, respectively. The extinction profiles were first divided by the measured AOD in order to normalize them to the optical depth. Polynomial curve fits were then applied to the normalized profiles to produce the vertical extinction models. Figure 13 displays the marine and polluted vertical extinction models. The marine model is given by

$$\frac{\sigma_M(z)}{\tau_A} = \begin{cases} -6.676\text{E}{-1}z^2 + 1.136\text{E}0z + 4.374\text{E}{-1} & z \le 0.55 \text{ km} \\ -2.821\text{E}{-2}z^3 + 3.250\text{E}{-1}z^2 - 1.220\text{E}0z + 1.495\text{E}0 & 0.55 > z \le 3.00 \text{ km} \\ 0 & z > 3.00 \text{ km} \end{cases} \quad (1)$$

and the polluted model is given by

$$\frac{\sigma_C(z)}{\tau_A} = \begin{cases} -7.533\text{E}-1z^2 + 1.219\text{E}0z + 4.364\text{E}-1 & z \le 0.40 \text{ km} \\ -3.320\text{E}-2z^3 + 2.747\text{E}-1z^2 - 9.053\text{E}-1z + 1.141\text{E}0 & 0.40 > z \le 3.00 \text{ km} \\ 0 & z > 3.00 \text{ km} \end{cases} \quad (2)$$

where $\sigma(z)$ is the extinction at altitude z (km), the M subscript denotes the marine model, the C subscript denotes the polluted model (from continental influence), and τ_A is the measured AOD. The standard deviations of the C1 and C4 extinction profiles and AOD were used to estimate how well the two models describe normalized extinction profiles actually measured during INDOEX. A spread of ± 65% was found for the model values at each altitude bin, and is indicated by the gray bars shown in Figure 13.

Based on the results from this cruise, neither the *Satheesh et al.* model or the polluted model would be correct during periods in the NH with a strong MBL inversion, and a surface air mass that was transported for several days over the ocean while the air mass above was directly from India. This is true even considering the rather large estimated error at each altitude of ± 65%. The models would also not accurately describe the profile found in the Arabian Sea. For these two conditions an increase in extinction above the MBL, peaking at approximately 2.4 km, would be required. It is beyond the scope of this study to accurately determine a model for these conditions due to uncertainty in the retrieved values of extinction in the C5 and C6 categories. More work is required in this area, and must include accurate measurements of extinction throughout the MBL and up to ~ 4km.

Appendix A

The measured MPL signal is raw data containing returns from molecules (Rayleigh scattering), aerosols, and clouds. The measured MPL signals also contain quantities associated with background noise, and instrument effects. The measured MPL signal, $P_{MPL}(r)$, is given by,

$$P_{MPL}(r) = \left\{ \frac{CO(r)E}{r^2} \left[\beta_R(r) + \beta_P(r) \right] \exp\left[-2\int_0^z \sigma_R(r')dr' \right] \exp\left[-2\int_0^z \sigma_P(r')dr' \right] \right\} + N_b + A(r) \qquad (A1)$$

where $P_{MPL}(r)$ is the lidar signal at range r (m), $\beta(r)$ is the backscatter coefficient $(m\,sr)^{-1}$ at range r, $\sigma(r)$ is the extinction coefficient $(m)^{-1}$ at range r, the R subscript denotes a Rayleigh quantity (due to molecular scattering), and the P subscript denotes a particle (aerosols, clouds) quantity. C is the MPL system constant (principally a function of the optics). E, is proportional to the pulse output energy, and N_b is background noise due to sunlight at 523 nm. $O(r)$ (overlap function), and $A(z)$ (afterpulse function) are instrument effects and are discussed later in the Appendix.

All Rayleigh quantities in the MPL signal are considered known because of the accuracy current models have achieved in calculating molecular scattering and absorption. S_R is a constant, and $\beta_R(r)$ and $\sigma_R(r)$ are constructed using tables published in *McClatchey et al.* [1972] for tropical, mid-latitude (winter/summer), and sub-arctic (winter/summer) atmospheres.

Extinction-Backscatter Ratio

Extinction and backscatter are related using the extinction-backscatter ratio (units of sr),

$$S_i = \frac{\sigma_i(r)}{\beta_i(r)} \qquad (A2)$$

where S_i is the extinction-backscatter ratio, and the i subscript indicates a Rayleigh or particle quantity. The extinction-backscatter ratio can also be related to ω_o, the single scatter albedo, and $P_i(180)$, the phase function at 180° (normalized to 4π), by the following equation,

$$S_i = \frac{4\pi}{\omega_o P_i(180)} \tag{A3}$$

S_R is a constant and is equal to $8\pi/3$. S_P, henceforth referred to as the S-ratio, is unknown but typically ranges in value from 10 to 100 sr [*Spinhirne et al.*, 1980; *Ackermann*, 1998; *Doherty et al.*, 1999; *Welton et al.*, 2000; *Ansmann et al.*, 2000; *Voss et al.*, 2001] for aerosols. In this study, the S-ratio is treated as constant with respect to range through an aerosol layer. The S-ratio of each individual layer will change depending upon the single scatter albedo and phase function of the aerosols and/or clouds in the layer. Errors from using an assumption of range constant S-ratios in analysis of MPL data are discussed in *Welton* [1998] and *Welton et al.* [2000], and also in Section 4.

Signal Corrections

The raw signal in Eq. (A1) is not in a mathematical format suitable for use in lidar algorithms. Also, the following instrument-related quantities in the raw signal are not related to returns from molecules, aerosols, or clouds: C, E, O(r), and A(r). These quantities must be removed from the raw MPL signals before analysis can be performed. The first step in the correction process is to subtract N_b, and then to normalize Eq. (A1) by multiplying by r^2 and dividing by E.

Afterpulse, A(r), is detector noise and is caused by turning on the detector prior to triggering the laser pulse. The initial signal spike on the detector causes the release of photoelectrons from the photodiode detector with time. The photoelectrons released during this process are recorded as an apparent signal (afterpulse), which is not associated with the true

signal returns from the atmosphere. Afterpulse is determined by measuring the normalized signal when the MPL laser pulses are completely blocked prior to the first range bin. In this arrangement, the signal does not contain any return from the atmosphere and the measured signal is the normalized afterpulse (range corrected and energy normalized). The afterpulse is measured over 20 minutes and the average is used to correct the field measurements. The standard deviation during this period is used as a measure of the afterpulse error. To perform the afterpulse correction, the normalize afterpulse function is subtracted from the normalized signal.

The overlap function, $O(r)$, is a multiplicative instrument effect and is due to the difference between the field-of-view of the transmit and receive paths in the MPL. Overlap causes a reduction in signal strength within the overlap range (typically ~ 4 to 5 km) because the MPL cannot accurately image the incoming signals. The overlap problem must be corrected in order to analyze boundary layer aerosols using a lidar system. Our overlap correction is similar to work presented in *Sasano et al.* [1979]. Using vertically oriented lidar data, they assume that the atmosphere is constant through their overlap region (300 m), and then divide the affected signals by the signal at 300 m to calculate an overlap function. Our overlap range is much further than 300 m, and an assumption of atmospheric homogeneity in the vertical is not possible. It is much more likely to have the required homogeneity along a horizontal line of sight. Therefore, our overlap correction process involves acquiring MPL data while the instrument is oriented horizontally. When plotting the natural logarithm of the normalized and afterpulse corrected MPL signal versus range, one should obtain a linear relationship at distances greater than the overlap range (where $O(r)$ is = 1). The overlap function will be less than 1 for distances less than the overlap range, and the signal strengths are decreased. $O(r)$ is determined by first performing a linear fit to in the region where the overlap is 1 ($r >$ overlap range). $O(r)$ is calculated by

forcing the measured data to equal the fit line in the region $r <$ overlap range, because the fit line represents what the measured data should be in the near range (assuming horizontal homogeneity). The error in the calculated overlap is a function of the standard deviation of the measured signals, the afterpulse error, and error in the linear fit. The overlap error equation is not shown here for brevity. Finally, to correct the measured signals for overlap problems, the normalized and afterpulse corrected signal is divided by $O(r)$.

The signal resulting from the correction process is referred to as normalized relative backscatter, $P_{NRB}(r)$, also known as NRB, is given by,

$$P_{NRB}(r) = C[\beta_R(r) + \beta_P(r)]\exp\left[-2\int_0^r \sigma_R(r')dr'\right]\exp\left[-2\int_0^r \sigma_P(r')dr'\right] \quad . \tag{A4}$$

$P_{NRB}(r)$ is proportional to the total backscatter coefficient at range r, and is attenuated by the squared transmission (exponential terms combined) from 0 to range r. The term relative is used because an instrument parameter, C, is the proportion constant. Error in the NRB signals is a function of both the afterpulse and overlap errors (the equation is not shown here for brevity).

Calibration

Calibration involves determination of the lidar system constant, C, and should be performed routinely during a measurement campaign. C is determined during situations where all aerosols are contained within the boundary layer and where there is also a cloud free section of air well above the top of the boundary layer. This region is termed the calibration zone.

A 1 km deep calibration zone is identified using the following criteria. The NRB signal throughout the calibration zone must have a good signal-to-noise ratio. It is not possible to determine C accurately if the NRB signal errors in the calibration zone are large. Also, the NRB signals must decrease with range throughout the calibration zone in the same manner as expected

for a Rayleigh-only NRB signal (calculated using modeled Rayleigh terms). If these conditions are met then the calibration zone is assumed to have $\beta_P(r) = 0$ at all ranges in the zone.

C is calculated directly from the lidar signals in the calibration zone after determining the transmission. The transmission is a function of the Rayleigh optical depth (known) and the aerosol optical depth (AOD) from the MPL altitude to the calibration altitude. The AOD is input from an independent measurement using a sunphotometer. C is calculated at each range bin in the calibration zone using the following equation,

$$C(r) = \frac{P_{NRB}(r)}{\beta_R(r)} \exp[2\tau_A] \exp\left[2\int_0^r \sigma_R(r')dr'\right] \qquad (r_1 \le r \le r_2) \tag{A5}$$

where $C(r)$ is the calculated calibration constant at each range bin in the calibration zone, r_1 is the bottom of the calibration zone, r_2 is the top of the calibration zone, τ_A is the independent AOD measurement, and $P_{NRB}(r)$ is typically about a 10 minute signal average. The values of $C(r)$ are averaged to produce a final value for C. Periodic calibrations must be made during cloud-free periods of an experiment and a linear interpolation is used to generate values of C for any time during the experiment. The NRB signals are calibrated by dividing them by C.

The error in C is termed ΔC and is calculated using the following equation

$$\Delta C = C\sqrt{\left[\frac{\Delta P_{NRB}}{P_{NRB}}\right]^2 + \left[\frac{\Delta\beta_R}{\beta_R}\right]^2 + \left[\frac{\Delta T_R^{\,2}}{T_R^{\,2}}\right]^2 + \left[\frac{\Delta T_A^{\,2}}{T_A^{\,2}}\right]^2} \tag{A6}$$

where ΔP_{NRB} is the combined NRB error and deviation in the measured signals during the calibration time period, $\Delta\beta_R$ is the error in the Rayleigh backscatter value, $\Delta T_R^{\,2}$ is the error in the Rayleigh transmission-squared term (first exponential in Eq.(A4)), and $\Delta T_A^{\,2}$ is the error in the aerosol transmission-squared term (second exponential in Eq.(A4)). The maximum error for both Rayleigh terms was estimated by using a comparison of the two extreme Standard Atmosphere models. The tropical and sub-arctic-winter atmospheres were averaged to produce a model

Rayleigh profile. The deviation between the average model and the two extreme atmospheres was used to determine the maximum error for both $\Delta\beta_R$ and ΔT_R^2. The results are considered the maximum expected errors since in reality the correct atmospheric model model is obtained far more accurately then our model assumed. The results [unpublished data] showed that the maximum error due to both Rayleigh terms combined was less then 2% at typical MPL calibration altitudes (approximately 6 to 8 km). The error in the ΔT_A^2 term is calculated using error bars on the measured AOD. The final ΔC for both MPL systems during INDOEX 1999 was calculated to be $\pm$ 5% using the NRB error during the calibration measurements, the measured AOD error bars, an assumed total Rayleigh induced error of 1%, and an additional small error from the linear fit function used to determine *C*.

Cloud Screening

The calibrated signals, referred to as attenuated backscatter, were then cloud screened by removing any signals with values greater than 0.8 $(km\ sr)^{-1}$ below the calibration zone. The cloud screen limit was chosen using the following procedure. True cloud lidar signal returns were identified a number of times throughout the cruise by comparing the lidar signals with images from a co-located upward viewing time-lapse camera (roughly bore-sighted to the MPL view angle). The average signal return from the clouds was used as the cloud screen limit given above.

MPL Data Products

The cloud screened attenuated backscatter signals were averaged over 30 minute periods on the ship, and 10 minute periods at KCO, and then used to determine the final data products. The following MPL Data products specific to this study include:

- top-of-the-marine-boundary-layer (MBL Top), units in km
- top of the highest aerosol layer detected (Top Height), units in km

- aerosol optical depth (AOD) at 523 nm (from 0 km to the top height)
- aerosol extinction-to-backscatter ratio (S-ratio) at 523 nm, units in sr
- profiles of aerosol extinction (σ) at 523 nm, units in km^{-1}

Error bars are produced for each data product using ΔC, and signal noise determined by the standard deviation of the signal time average. Signal noise is due to a combination of fluctuations in the aerosol properties during the time average, and the signal-to-noise ratio which is dependent upon the background sunlight level and laser energy output.

Throughout the experiment, the AOD of each cloud-screened signal average was calculated directly from signals in a particle-free layer of air above the lower troposphere. The layer was identified in the same fashion as used to pick the calibration zone. The AOD is calculated from the signals in the new zone by simply inverting Eq. (A5) to solve for the AOD.

Aerosol layer heights were then determined. The layer detection algorithm is based on comparisons between the measured signal strength and the value of a calculated Rayleigh lidar signal that has been attenuated by the measured AOD. The top height is found be searching downward, one altitude bin at a time, from the calibration zone until a point when the measured signal strength is greater than the Rayleigh signal by a predetermined threshold setting. This altitude bin is identified as a possible top height. The signal average over the next 500 m is then compared to the Rayleigh signal in order to avoid false determinations caused by signal noise. If the comparison passes, then the initial altitude bin is termed the top height. The MBL top is found by searching upward from the surface, and computing the percent difference between the measured signal and the Rayleigh signal. If this value changes by more than a predetermined threshold between successive altitude bins, then the lower bin is identified as a possible MBL top. A similar signal average is conducted over the next 500 m (upward this time) to avoid false

identification of the MBL top due to signal noise. If the comparison passes, then the initial altitude bin is termed the MBL top. During INDOEX a 5% threshold setting was used for detecting the top height and a threshold setting of 50% was used to detect the MBL top. The thresholds were obtained based on prior experience during an earlier cruise [*Voss et al.*, 2001].

The extinction profile and the S-ratio are determined last using the inversion procedure discussed in *Welton et al.* [2000]. The pre-determined AOD is used to constrain the inversion and is used to calculate the S-ratio and then the backscatter profile. After determining the backscatter profile, the extinction profile is generated by multiplying the backscatter values by the S-ratio. For situations containing both a MBL and aerosol above, the two layers can only be treated separately if there is an aerosol-free layer of air at least 1 km long between the two layers. The latter did not occur during INDOEX, and therefore the extinction profile for both the MBL and above had to be calculated together by assuming that the S-ratio is constant with altitude from the surface to the top height. Errors induced using a constant S-ratio are discussed further in *Welton et al.* [2000] and in section 4.

Baseline errors for the data products were estimated using only ΔC and error propagation of each term through the algorithm process. The estimated baseline error for the AOD was $\pm$ 0.02 for the MPL systems, and the baseline error in determining aerosol layer heights is estimated at $\pm$ 0.075 km. The baseline error for extinction values in a profile is estimated to be $\pm$ 0.005 km^{-1}, and $\pm$ 5 sr for the S-ratio. The actual error bars on individual measurements may be larger than the baseline errors due to signal noise.

Acknowledgments

The authors wish to thank the crew of the NOAA ship R/V Ronald H. Brown and the staff at KCO for their outstanding support during the experiment. We also wish to thank Piotr Flatau for help in organizing lidar measurements on the ship, for providing time-lapse camera sky images, and helpful comments on the paper. We also thank Xu Li-Jones for operating the KCO MPL system during INDOEX. Finally, we thank the governments of Mauritius and The Maldives for allowing us to sample within their territorial waters. Micro-pulse lidar measurements onboard the R/V Ronald H. Brown were funded by the NASA SIMBIOS project and the NASA-MODIS contract NA55-31363, and an MPL system was provided by the CERES Surface Validation Group at NASA LaRC. Micro-pulse lidar measurements at KCO were supported by the NSF-funded Center for Clouds, Chemistry, and Climate as part of the INDOEX program and the NOAA Office of Oceanic and Atmospheric Research. This research was also funded in part by the Aerosol Program of the NOAA Climate and Global Change Program and NASA Global Aerosol Climatology Project (PKQ).

References

Ackermann, J., The Extinction-to-Backscatter Ratio of Tropospheric Aerosol: A Numerical Study, *J. Atmos. Oceanic Tech.*, 15, 1043-1050, 1998.

Andrews, E., P. Sheridan, A. Jefferson, and J. Ogren, Measurements of the humidity-dependence of light scattering by aerosols over the Indian Ocean, *J. Geophys. Res.*, submitted, this issue.

Angstrom, A., The parameters of atmospheric turbidity, *Tellus*, 16, 64-75, 1964.

Ansmann, A., D. Althausen, U. Wandinger, K. Franke, D. Müller, F. Wagner, and J. Heintzenburg, Vertical profiling of the Indian aerosol plume with six-wavelength lidar during INDOEX: A first case study, *Geophys. Res. Lett.*, 27, 963-966, 2000.

Carrico, C. M., M. J. Rood, and J. A. Ogren, Aerosol light scattering properties at Cape Grim, Tasmania, during the first Aerosol Characterization Experiment (ACE 1), *J. Geophys. Res.*, 103, 16565-16574, 1998.

Coakley, J. A., B. Gandrud, T. Bates, A. Clarke, W. Collins, R. Dickerson, F. Dulac, J. Heintzenberg, T.N. Krishnamurti, A. Jayaraman, V. Ramanathan, R. Sardourny, and J. Williams, General Overview of INDOEX, *J. Geophys. Res.*, submitted, INDOEX special issue 1.

Crutzen, P. J., and V. Ramanathan, Indian Ocean Experiment: Foreword to the Special Issue, *J. Geophys. Res.*, submitted, INDOEX special issue 1.

Collins, W. D., P. J. Rasch, B. E. Eaton, B. Khattatov, J. F. Lamarque and C. S. Zender, Simulating aerosols using a chemical transport model with assimilation of satellite aerosol retrievals: Methodology for INDOEX, *J. Geophys. Res.*, submitted, 2000a.

Collins, W. D., P. J. Rasch, B. E. Eaton, E. J. Welton, and J. D. Spinhirne, Improvements in aerosol forecasts from assimilation of in situ and remotely sensed aerosol properties, *J. Geophys. Res.*, submitted, INDOEX special issue 1.

Doherty, S. J., T. L. Anderson, and R. J. Charlson, Measurements of the lidar ratio for atmospheric aerosols with a 180 backscatter nephelometer, *Appl. Optics*, 38, 1823-1832, 1999.

Dickerson, R. R., J. P. Burrows, L. Granat, S. Guazzotti, A. Hansel, J. E. Johnson, C. Neususess, P. K. Quinn, D. Savoie, E. J. Welton, V. Wagner, and A. Zahn, Overview: The Cruise of the Research Vessel Ronald H. Brown during the Indian Ocean Experiment (INDOEX) 1999, *J. Geophys. Res.*, submitted, this issue.

Draxler, R. R., and G. D. Hess, Description of the Hysplit_4 modeling system, *NOAA Tech. Memo. ERL ARL-224*, 1997.

Fernald, F. G., Analysis of atmospheric lidar observations: some comments, *Appl. Opt.*, 23, 652-653, 1984.

Fitzgerald, J. W., Model of the aerosol extinction profile in a well-mixed marine boundary layer, *Appl. Opt.*, 28, 3534-3538, 1989.

Holben, B.N., Eck, T.F., Slutsker, I., Tanre, D., Buis, J.P., Setzer, A., Vermote, E., Reagan, J.A., Kaufman, Y.J., Nakajima, T., Lavenu, F., Jankowiak, I., and A. Smirnov, AERONET-A federated instrument network and data archive for aerosol characterization, *Rem. Sens. Environ.* 66, 1-16, 1998.

Krishnamurti, T. N., B. Jha, J. Prospero, A. Jayaraman, and V. Ramanathan, Aerosol and pollutant transport and their impact on radiative forcing over the tropical Indian Ocean during the January-February 1996 pre-INDOEX cruise, *Tellus*, 50B, 521-542, 1998.

Lobert, J. M., V. Ramanathan, J. Prospero, and A. Majeed, Kaashidhoo Climate Observatory (KCO): A new site for observing long-term changes in the tropical Indian Ocean, *J. Geophys. Res.*, submitted, INDOEX special issue 1.

Meywerk, J., and V. Ramanathan, Observations of the spectral clear-sky aerosol forcing over the tropical Indian Ocean, *J. Geophys. Res.*, 104, 24359-24370, 1999.

Mishchenko, M. I., L. D. Travis, R. A. Kahn, and R. A. West, Modeling phase functions for dust-like tropospheric aerosols using a shape mixture of randomly oriented polydisperse spheriods, *J. Geophys. Res.*, 102, 16831-16847, 1997.

Palm, S., W. Hart, D. Hlavka, E. J. Welton, and J. D. Spinhirne, Geoscience Laser Altimeter System (GLAS) Atmospheric Data Products: Algorithm Theoretical Basis Document Version 4.1, Available from NASA Goddard Space Flight Center, Code 912, Greenbelt, MD, 20771, USA, 2001.

Quinn, P. K., T. S. Bates, D. J. Coffman, T. L. Miller, J. E. Johnson, C. Neususess, E. J. Welton, and P. Sheridan, Variability in Aerosol Optical Properties during INDOEX and Controlling Factors, *J. Geophys. Res.*, submitted, this issue.

Rajeev, K., V. Ramanathan, and J. Meywerk, Regional aerosol distribution and its long-range transport over the Indian Ocean, *J. Geophys. Res.*, 105, 2029-2043, 2000.

Russell, L. M., D. H. Lenschow, K. K. Laursen, P. B. Krummel, S. T. Siems, A. R. Bandy, D. C. Thornton, and T. S. Bates, Bidirectional mixing in an ACE 1 marine boundary layer overlain by a second turbulent layer, *J. Geophy. Res.*, 103, 16411-16432, 1998.

Sasano, Y., H. Shimizu, N. Takeuchi, and M. Okuda, Geometrical form factor in the laser radar equation: an experimental determination, *Appl. Opt.*, 18, 3908-3910, 1979.

Satheesh, S. K., V. Ramanathan, Xu Li-Jones, J. M. Lobert, I. A. Podgorny, J. M. Prospero, B. N. Holben, and N. G. Loeb, A model for the natural and anthropogenic aerosols over the tropical Indian Ocean derived from Indian Ocean Experiment data, *J. Geophys. Res.*, 104, 27421-27440, 1999.

Spinhirne, J. D., J. A. Reagan, and B. M. Herman, Vertical Distribution of Aerosol Extinction Cross Section and Inference of Aerosol Imaginary Index in the Troposphere by Lidar Technique, *J. Appl. Meteor.*, 19, 426-438, 1980.

Spinhirne, J. D., Rall, J., and V. S. Scott, Compact eye-safe lidar systems. *Rev. Laser Eng.*, 23, 26-32, 1995.

Voss, K. J., E. J. Welton, P. K. Quinn, J. Johnson, A. Thompson, and H. R. Gordon, Lidar measurements during Aerosols99. *J. Geophys. Res.*, in press, 2001.

Welton, E.J., Measurements of Aerosol Optical Properties over the Ocean Using Sunphotometry and Lidar. *Ph.D. Dissertation*. University of Miami, Coral Gables, 1-150, 1998.

Welton, E. J., K. J. Voss, H. R. Gordon, H. Maring, A. Smirnov, B. Holben, B. Schmid, J. M. Livingston, P. B. Russell, P. A. Durkee, P. Formenti, and M. O. Andreae, Ground-based Lidar Measurements of Aerosols During ACE-2: Instrument Description, Results, and Comparisons with other Ground-based and Airborne Measurements, *Tellus*, 52B, 635-650, 2000.

Figure Captions

Figure 1. Cruise track of the NOAA ship R/V Ronald H. Brown during the INDOEX 1999 IFP.

Figure 2. Aerosol extinction profiles from the ship during Leg 1 of the cruise. The profiles were calculated using 30 minute, cloud screened, MPL signal averages.

Figure 3. Aerosol extinction profiles from the ship during Leg 2 of the cruise. The profiles were calculated using 30 minute, cloud screened, MPL signal averages.

Figure 4. The MBL top and top heights (a), the AOD (b), and the S-ratio (c), are plotted versus the day of year for the ship MPL data.

Figure 5. The MBL top and top heights (a), the AOD (b), and the S-ratio (c), are plotted versus latitude for the ship MPL data.

Figure 6. The top height (a), and the AOD (b), are plotted versus the day of year for the KCO MPL data.

Figure 7. The ship and KCO MPL derived top heights (a), and the corresponding AOD (b) are plotted versus day of year during the ship and KCO inter-comparison period. The ship MBL top is also shown in (a). The ship and KCO sunphotometer derived AOD are also shown in (b) for reference. The MPL and sunphotometer AOD from the same platform are not independent of each other, but AOD between different platforms are.

Figure 8. Air mass trajectories at 0.5, 2.5, and 5.5 km are shown for each category defined in the text. The C1, C2, C3, C5, and C6 trajectory patterns are shown in (a), and C4 trajectory patterns are shown in (b).

Figure 9. The average extinction profile for each air mass category is shown in (a), the humidity profile is shown in (b), and the temperature profile is shown in (c). Horizontal bars represent the standard deviation in each average profile.

Figure 10. The average MBL top and top heights for each air mass category are shown in (a), the AOD is shown in (b), and the S-ratio is shown in (c). The vertical bars represent the standard deviation in each average.

Figure 11. The average S-ratio for each air mass category is shown plotted versus humidity. Modeled S-ratios from *Ackermann* [1998] for continental, marine, and dust aerosols are also shown. The following measured S-ratio values are also shown: saharan dust during ACE-2 [*Welton et al.*, 2000], polluted Maldives measurements during INDOEX [*Ansmann et al.*, 2000], and finally both marine aerosols and biomass aerosols over the ocean during the Aerosols99 cruise [*Voss et al.*, 2001]. The *Ansmann et al.* measurements were obtained with Raman lidar, and are shown segmented according to altitude.

Figure 12. The extinction determined at the ship (19 m) from combined nephelometer and PSAP measurements is plotted versus the MPL derived extinction at 75 m for each air mass category.

Figure 13. Models of marine and polluted marine (continental influence) aerosol vertical distributions are shown. The models depict the change in height of the aerosol extinction at each altitude, divided by the total AOD.

Table 1. INDOEX Air Mass Categories

Category	Description of Regions	Day of Year	*Dickerson et al.* [this issue] *
C1	0.5 km – SHmE 2.5 km – SHmE 5.5 km – SHmE	(1) 55.0 – 56.0 (2) 56.5 – 57.5	(1) SHmE (2) SHmE
C2	0.5 km – SHmE 2.5 km – SHmE 5.5 km – from Surface level NHmE	(1) 56.0 – 56.5	(1) SHmE
C3	0.5 km – NHmE 2.5 km - SHmE 5.5 km – SHmE	(1) 57.5 – 58.5	(1) SHmE to NHcT
C4	0.5 km – NHcT 2.5 km – NHmE and NHcT 5.5 km – NHmE, NHcT, and SHmE	(1) 58.5 – 60.0 (2) 63.0 – 66.0 (3) 73.0 – 75.0	(1) NHcT (2) NHcT (3) NHcX
C5	0.5 km – NHcX 2.5 km - NHcT 5.5 km - NHcT	(1) 66.0 – 69.0 (2) 71.0 – 73.0	(1) NHcT to NHcX (2) NHcX
C6	0.5 km – Iran and Saudi Arabia 2.5 km – Saudi Arabia 5.5 km – Saudi Arabia	(1) 69.0 – 71.0	(1) NHcX

* See *Dickerson et al.* [this issue] for a description of the following terms:
SHmE: Southern Hemisphere, marine Equatorial
NHmE: Northern Hemisphere, marine Equatorial
NHcT: Northern Hemisphere, continental Tropical
NHcX: Northern Hemisphere, continental eXtra-tropical

Table 2. Results From Each Air Mass Category

Category	MBL Top (km) (mean ± std)	Top Height (km) (mean ± std)	AOD (mean ± std)	S-ratio (sr) (mean ± std)
C1	0.95 ± 0.30	3.48 ± 0.75	0.05 ± 0.03	33 ± 6
C2	0.69 ± 0.07	4.51 ± 1.37	0.08 ± 0.04	54 ± 9
C3	0.75 ± 0.00	3.50 ± 0.53	0.06 ± 0.03	48 ± 5
C4	0.61 ± 0.17	3.06 ± 0.44	0.26 ± 0.12	53 ± 14
C5	0.72 ± 0.25	3.48 ± 0.23	0.33 ± 0.10	43 ± 12
C6	0.72 ± 0.30	3.68 ± 0.42	0.15 ± 0.03	55 ± 14

Figure 1

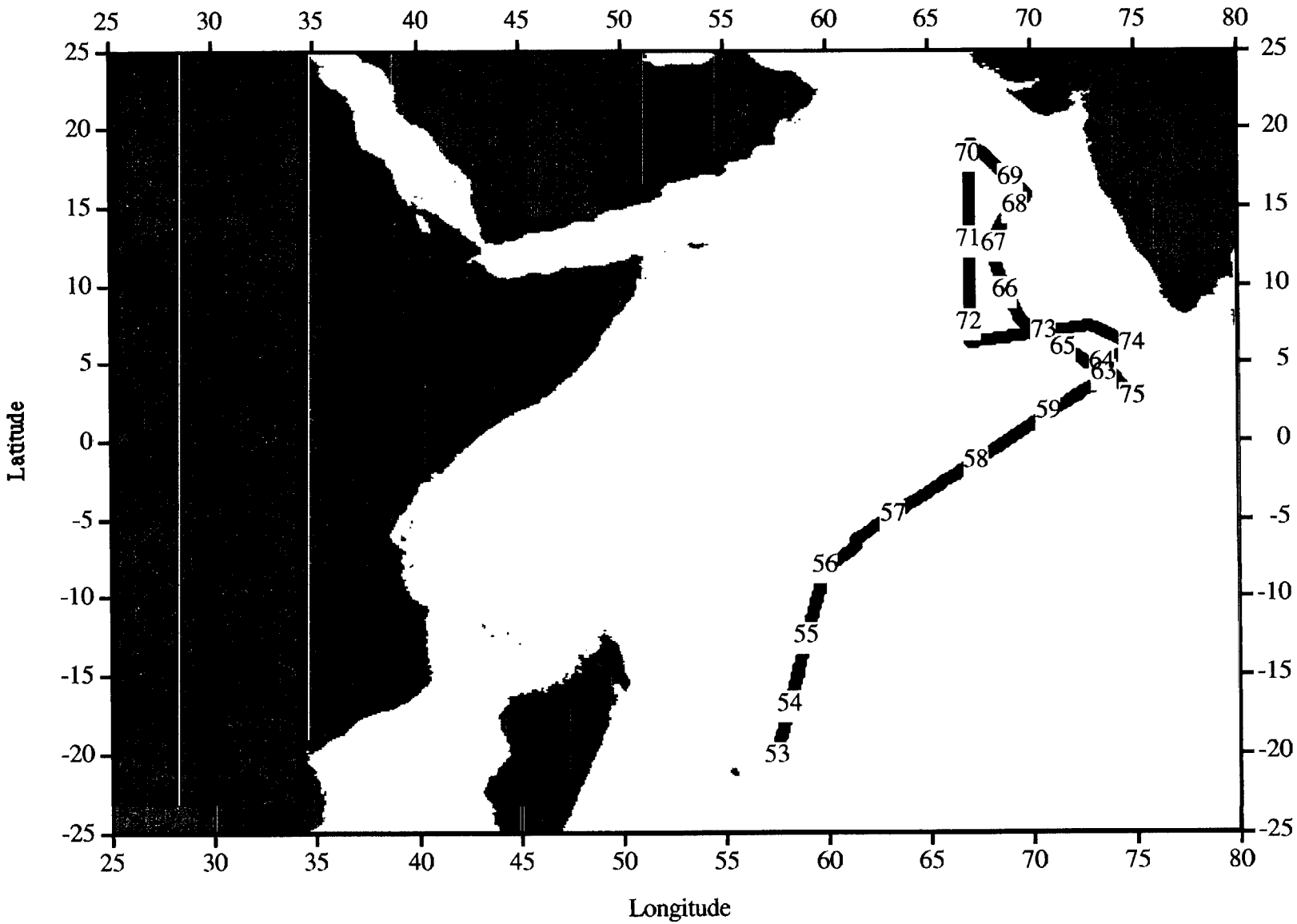
25
30
35
40
45
50
55
60
65
70
75
80
25
20
15
10
5
0
-5
-10
-15
-20
-25
Latitude
Longitude
70
69
68
71
67
66
72
73
74
65
64
63
75
59
58
57
56
55
54
53

Figure 2

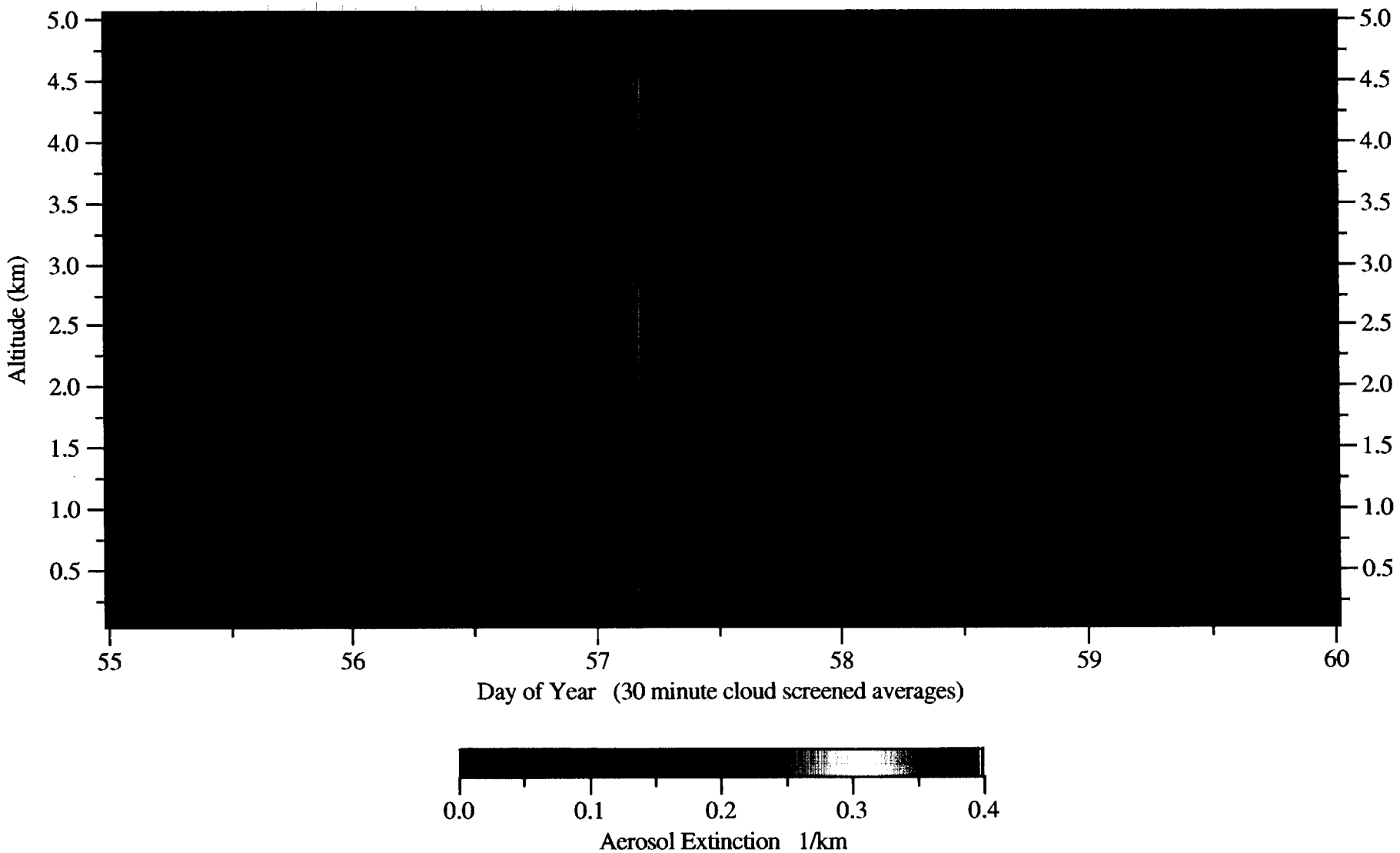
5.0
4.5
4.0
3.5
3.0
2.5
2.0
1.5
1.0
0.5
Altitude (km)
55
56
57
58
59
60
Day of Year (30 minute cloud screened averages)
0.0
0.1
0.2
0.3
0.4
Aerosol Extinction 1/km

Figure 3

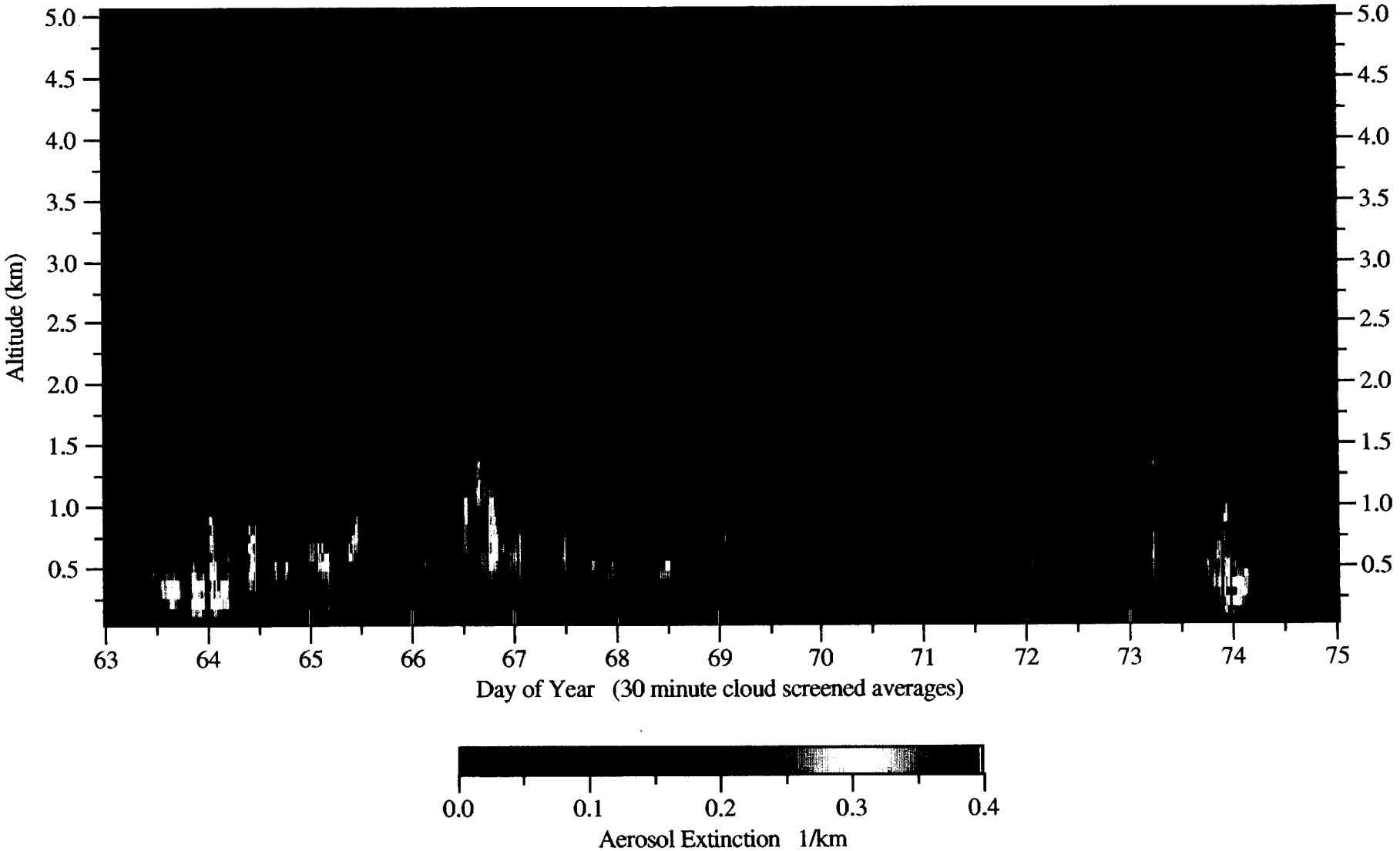
5.0
4.5
4.0
3.5
3.0
2.5
2.0
1.5
1.0
0.5
Altitude (km)
63
64
65
66
67
68
69
70
71
72
73
74
75
Day of Year (30 minute cloud screened averages)
0.0
0.1
0.2
0.3
0.4
Aerosol Extinction 1/km

Figure 4

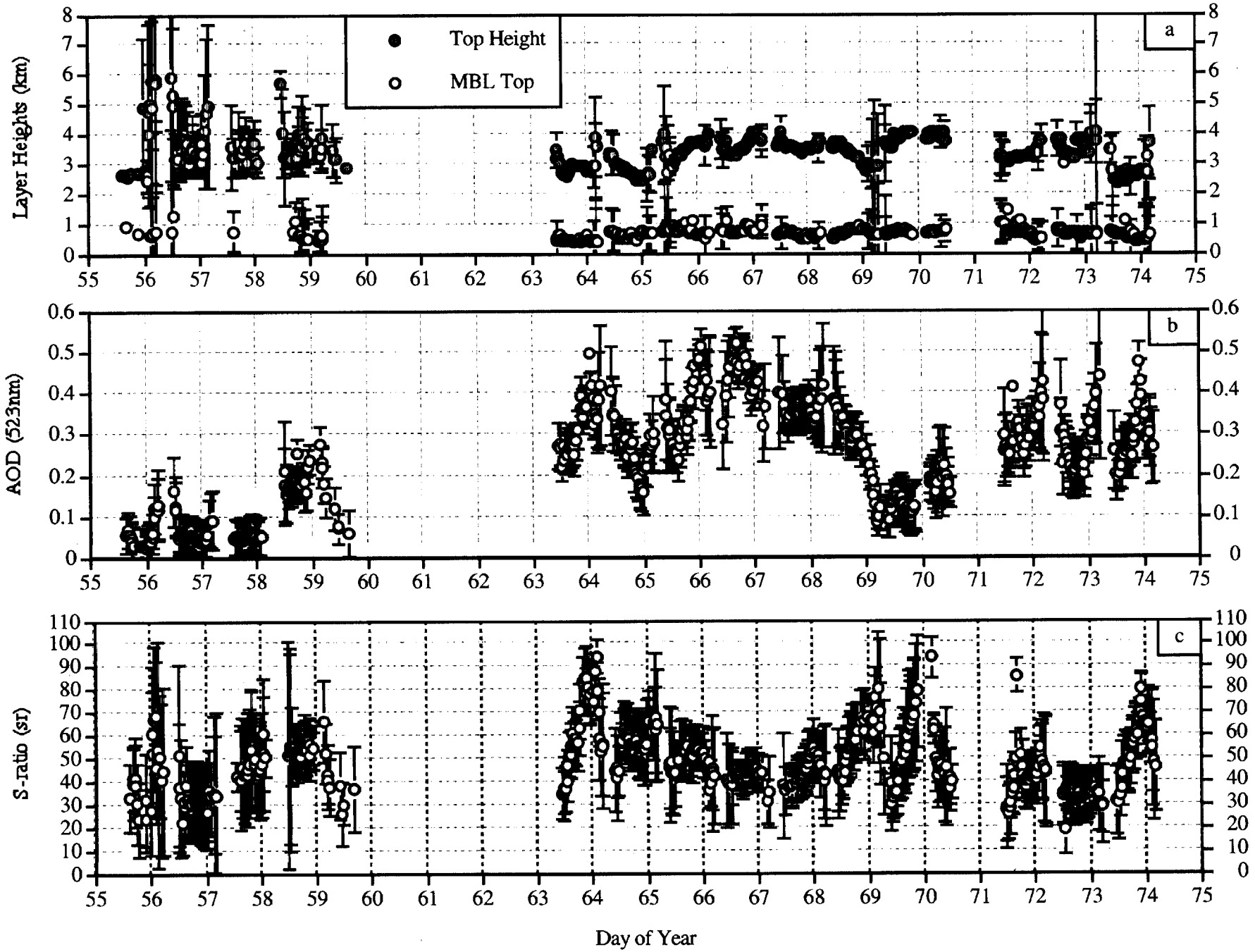
Top Height
MBL Top
a
b
c
Layer Heights (km)
AOD (523nm)
S-ratio (sr)
Day of Year

Figure 5

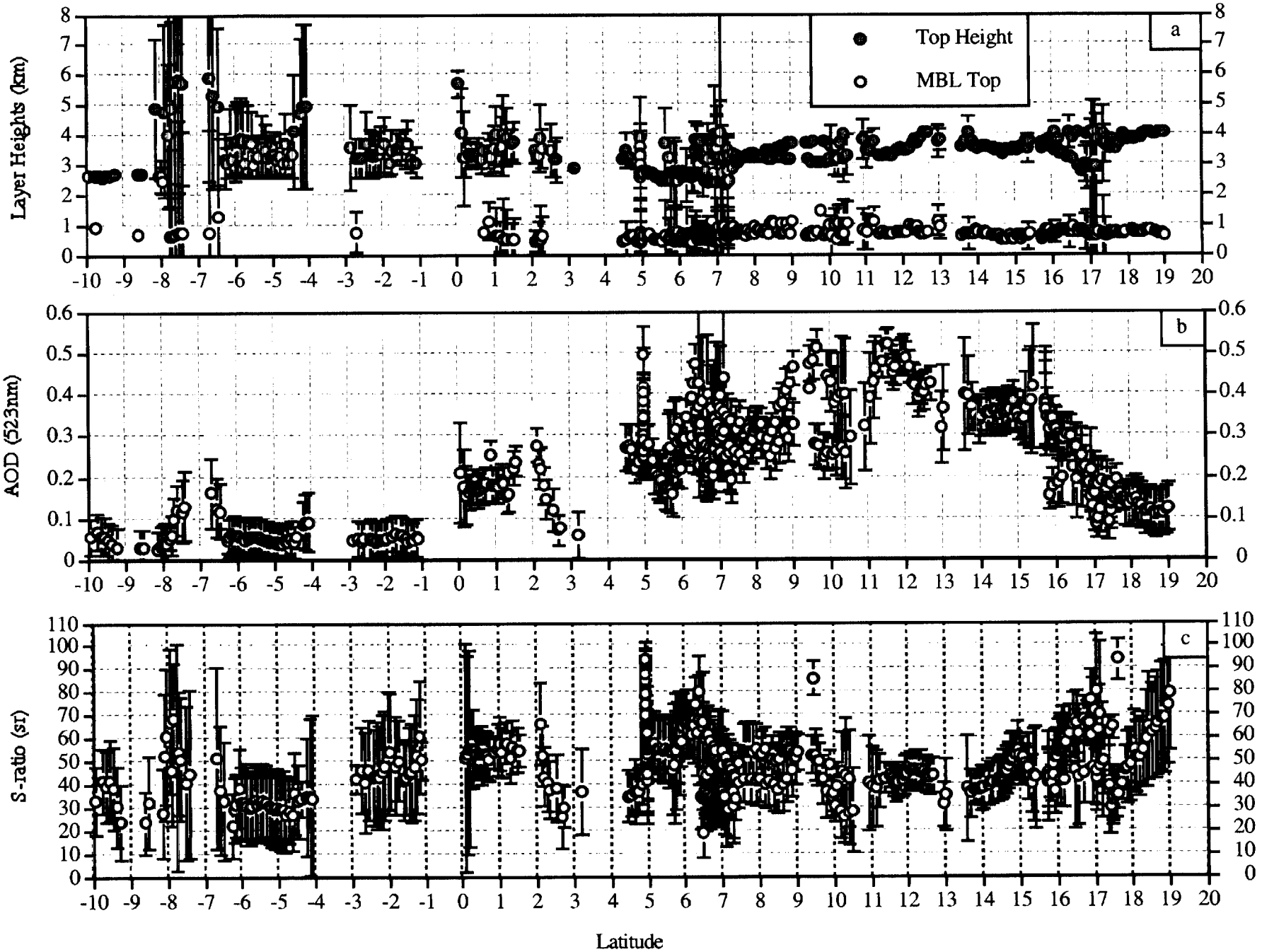
Layer Heights (km)
Top Height
MBL Top
a
AOD (523nm)
b
S-ratio (sr)
c
Latitude

Figure 6

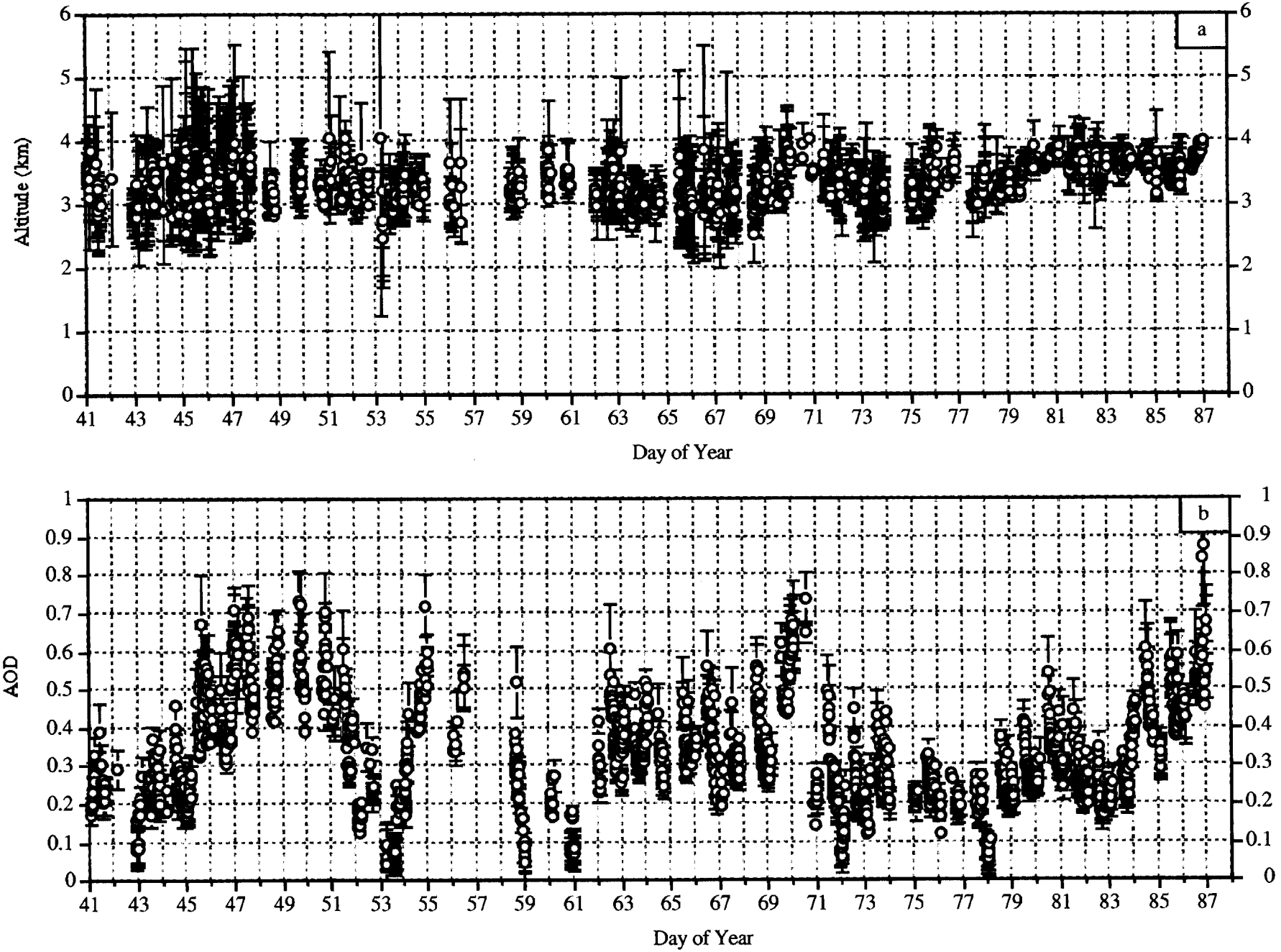
a
Altitude (km)
0
1
2
3
4
5
6
41 43 45 47 49 51 53 55 57 59 61 63 65 67 69 71 73 75 77 79 81 83 85 87
Day of Year
b
AOD
0
0.1
0.2
0.3
0.4
0.5
0.6
0.7
0.8
0.9
1
41 43 45 47 49 51 53 55 57 59 61 63 65 67 69 71 73 75 77 79 81 83 85 87
Day of Year

Figure 7

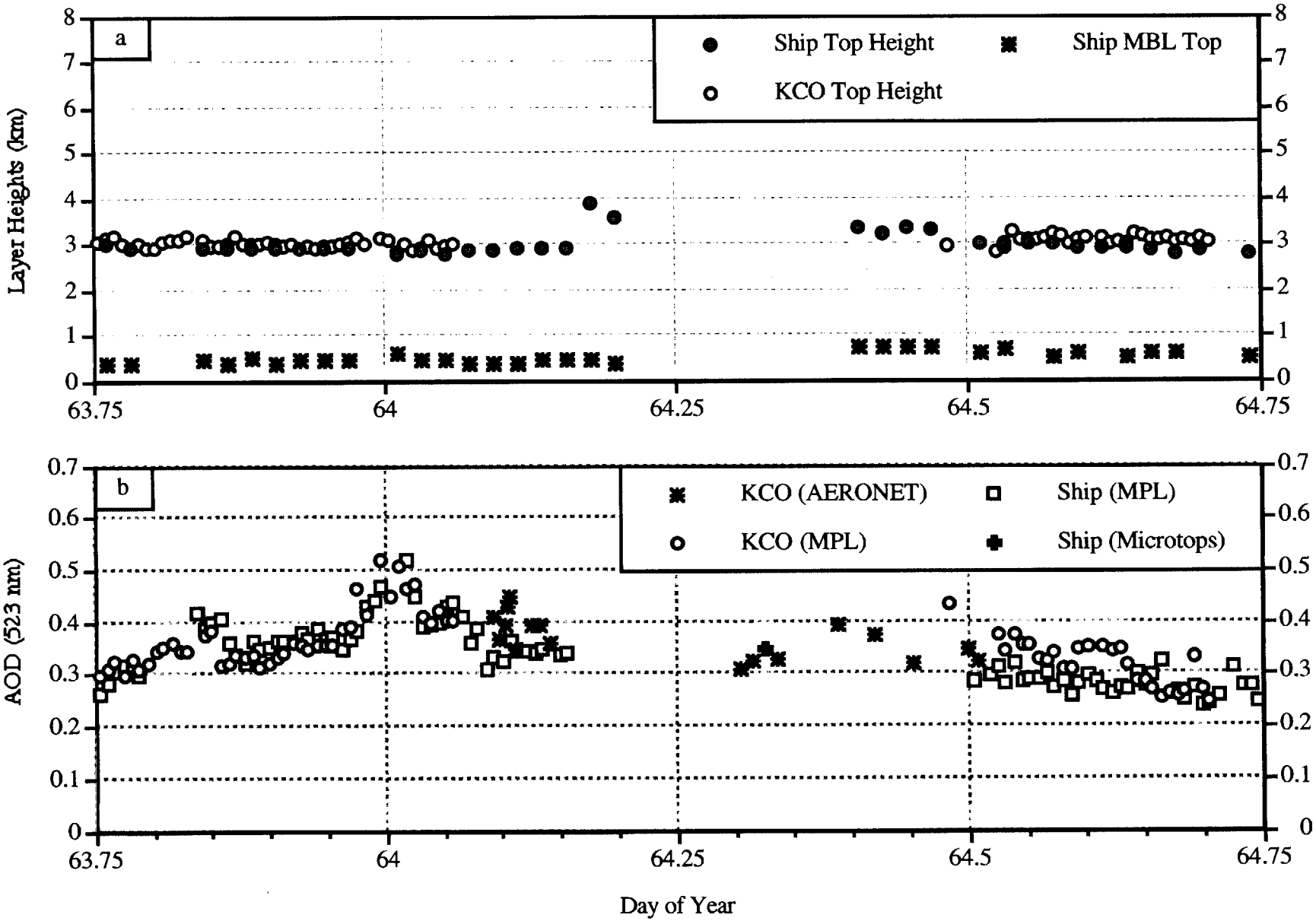
a
Ship Top Height
Ship MBL Top
KCO Top Height
Layer Heights (km)
0
1
2
3
4
5
6
7
8
63.75
64
64.25
64.5
64.75
b
KCO (AERONET)
Ship (MPL)
KCO (MPL)
Ship (Microtops)
AOD (523 nm)
0
0.1
0.2
0.3
0.4
0.5
0.6
0.7
63.75
64
64.25
64.5
64.75
Day of Year

Figure 8

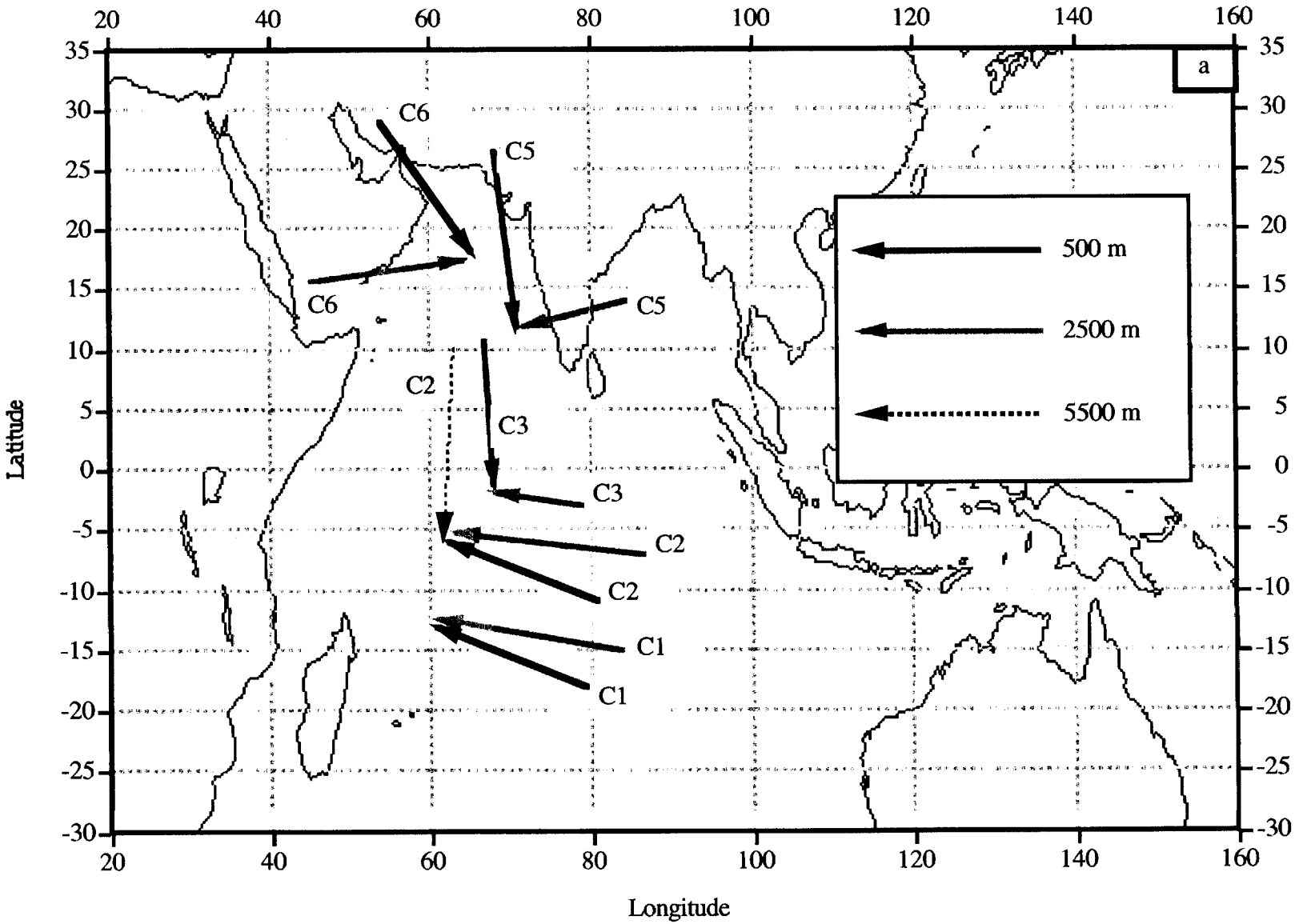
a
500 m
2500 m
5500 m
C6
C5
C2
C3
C1
Latitude
Longitude
20
40
60
80
100
120
140
160
35
30
25
20
15
10
5
0
-5
-10
-15
-20
-25
-30

Figure 8

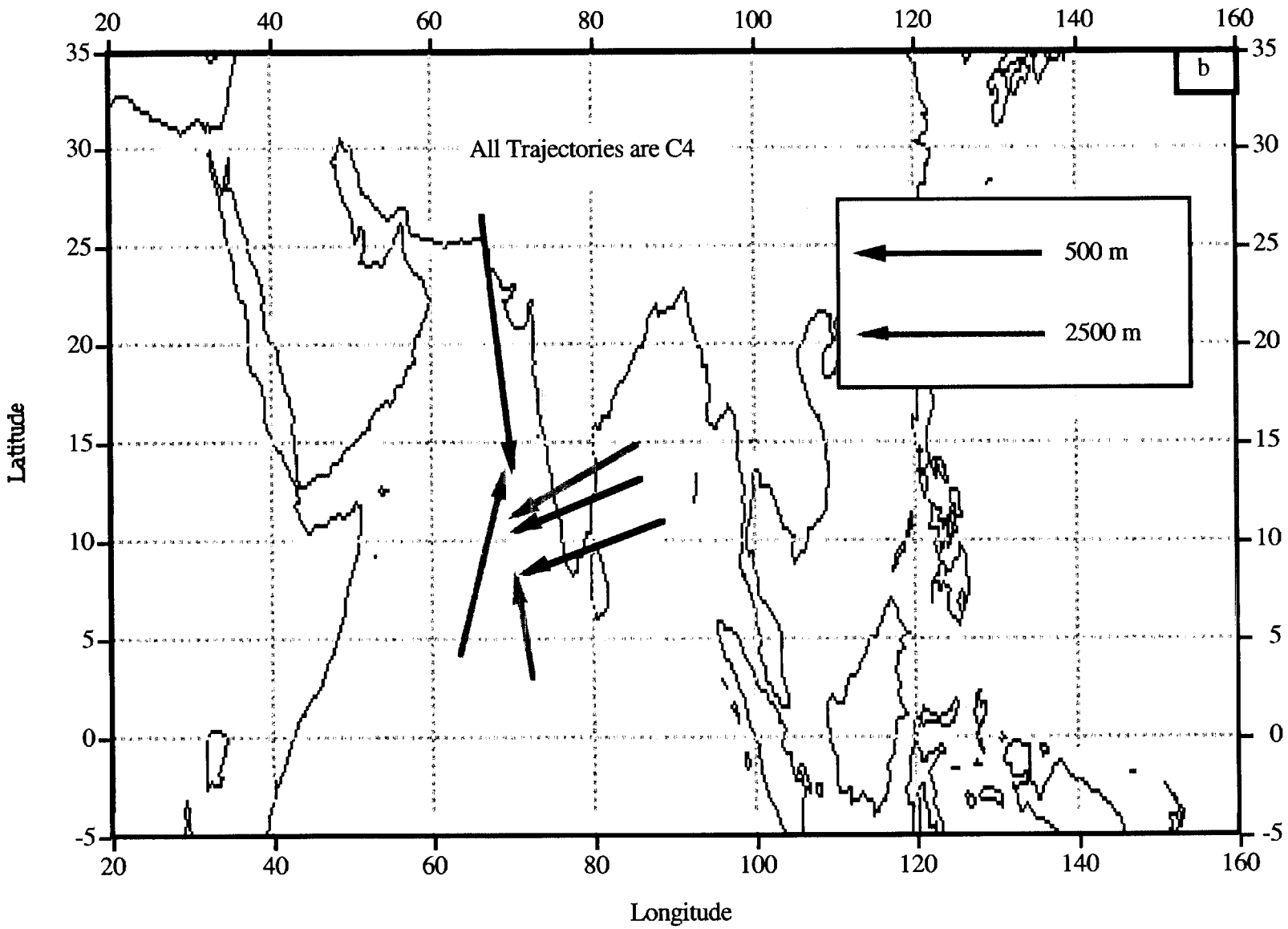
All Trajectories are C4
500 m
2500 m
b
Latitude
Longitude
20
40
60
80
100
120
140
160
35
30
25
20
15
10
5
0
-5

Figure 9

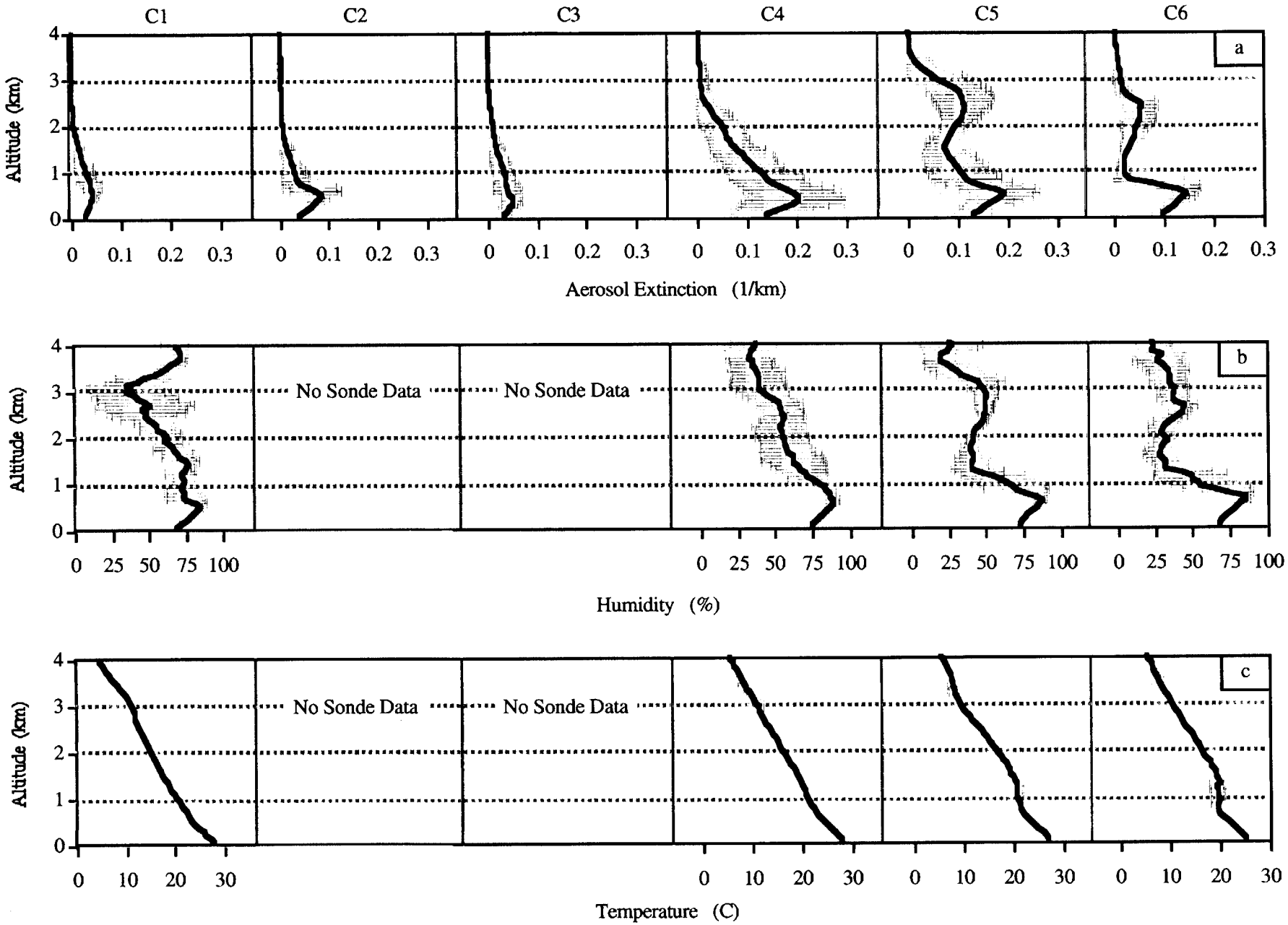
C1
C2
C3
C4
C5
C6
a
Altitude (km)
0
1
2
3
4
0 0.1 0.2 0.3
Aerosol Extinction (1/km)
b
No Sonde Data
No Sonde Data
0 25 50 75 100
Humidity (%)
c
No Sonde Data
No Sonde Data
0 10 20 30
Temperature (C)

Figure 10

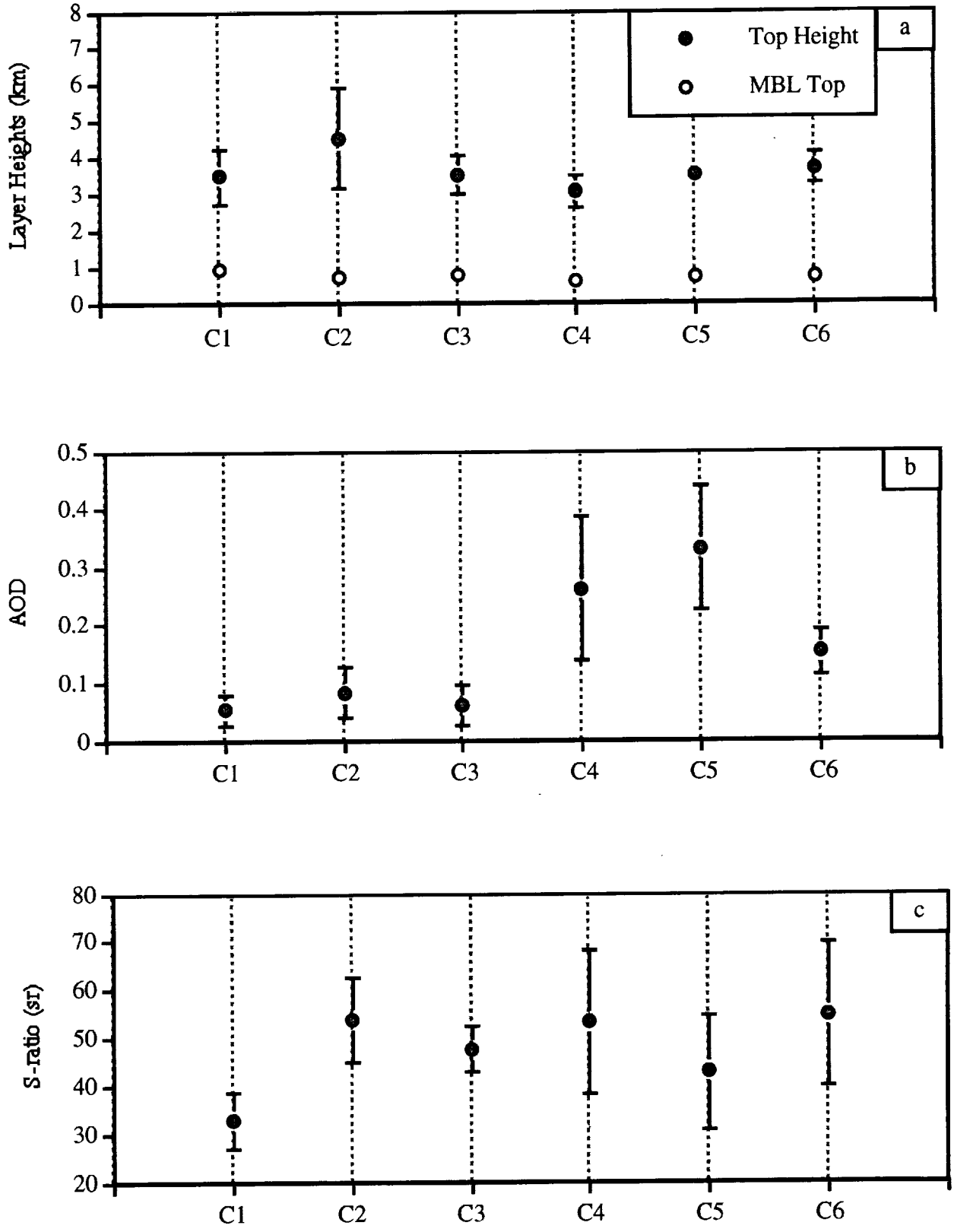
Layer Heights (km)
Top Height
MBL Top
a
C1
C2
C3
C4
C5
C6
AOD
b
S-ratio (sr)
c

Figure 11

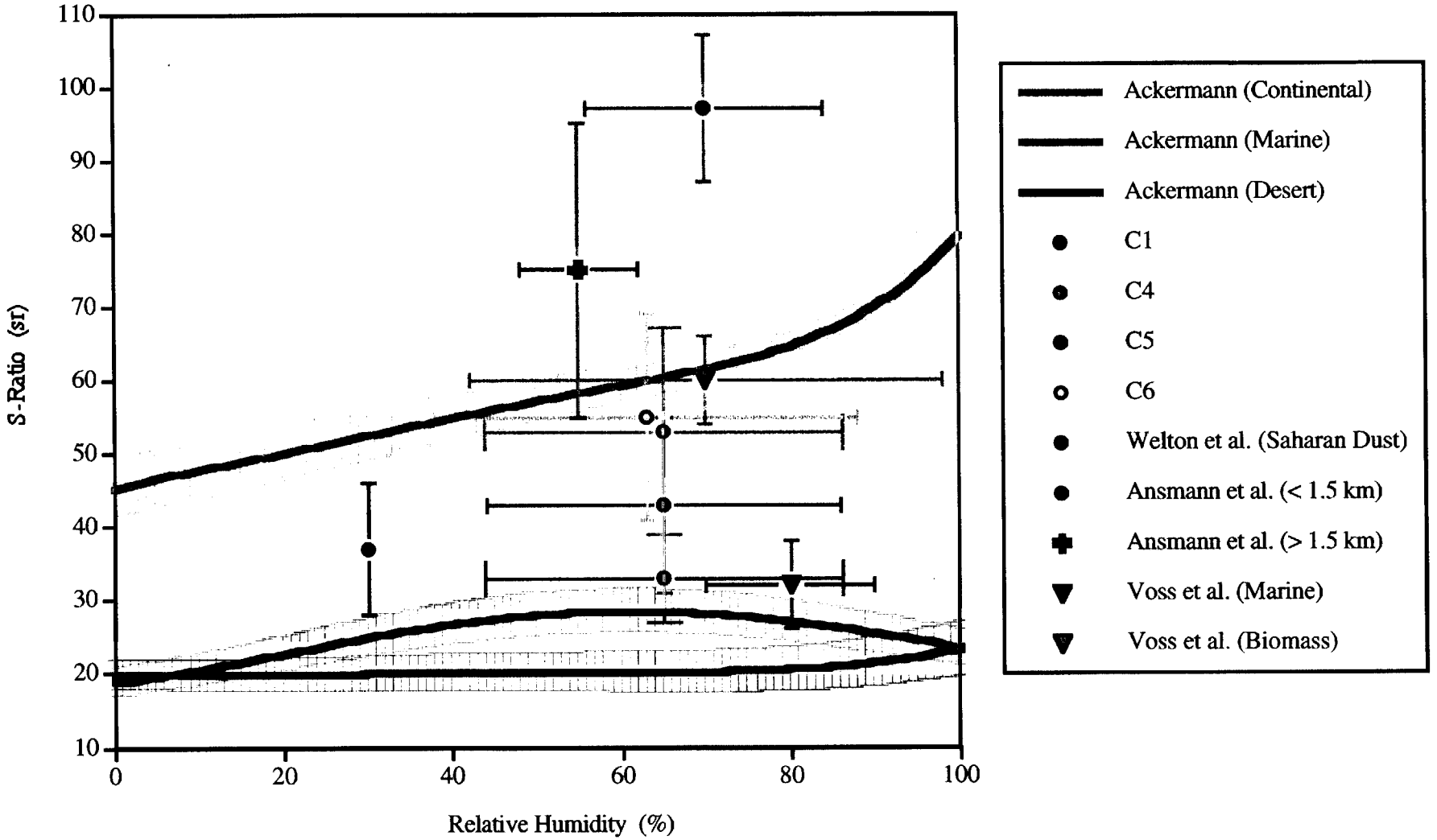
110
100
90
80
70
60
50
40
30
20
10
S-Ratio (sr)
0
20
40
60
80
100
Relative Humidity (%)
Ackermann (Continental)
Ackermann (Marine)
Ackermann (Desert)
C1
C4
C5
C6
Welton et al. (Saharan Dust)
Ansmann et al. (< 1.5 km)
Ansmann et al. (> 1.5 km)
Voss et al. (Marine)
Voss et al. (Biomass)

Figure 12

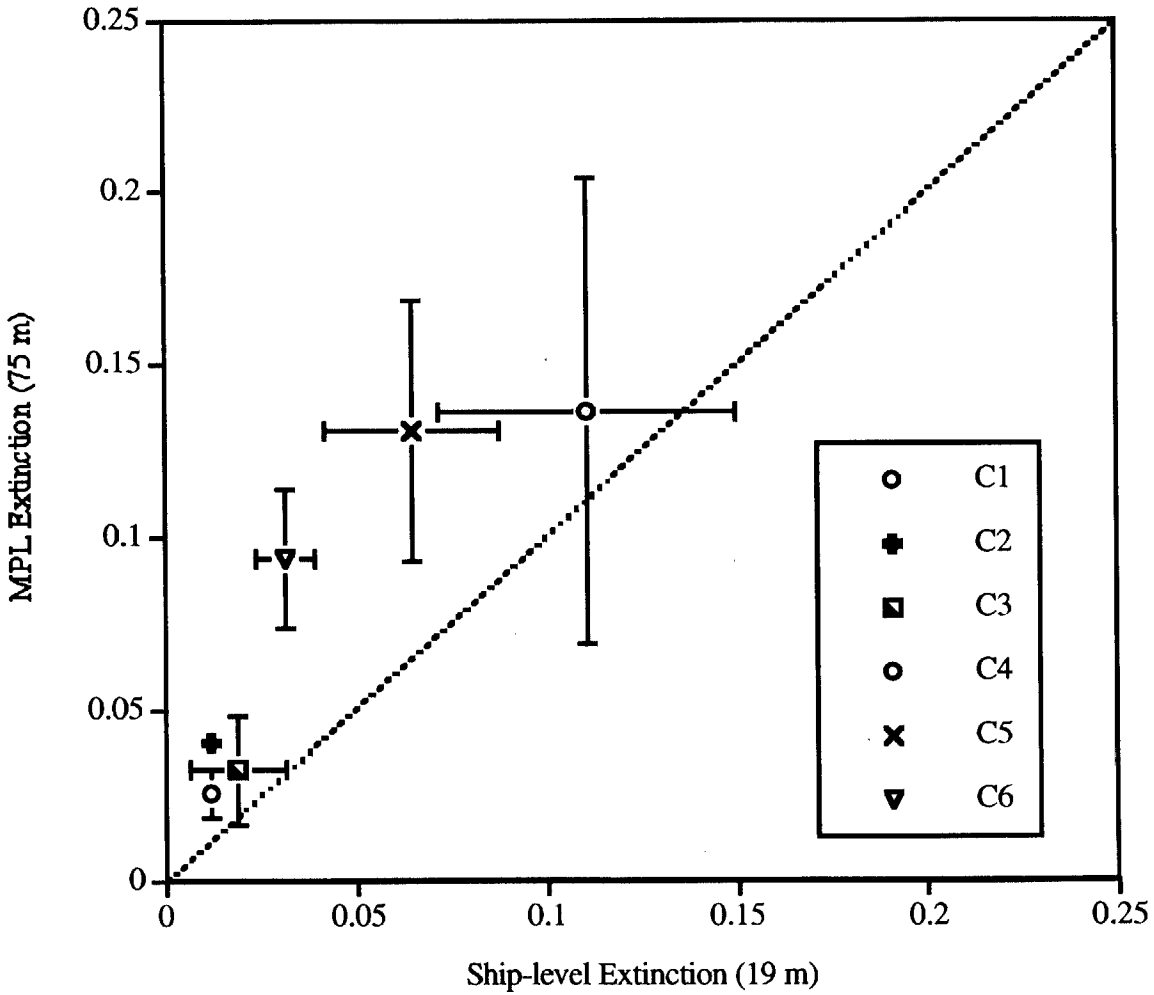
0.25
0.2
0.15
0.1
0.05
0
0
0.05
0.1
0.15
0.2
0.25
MPL Extinction (75 m)
Ship-level Extinction (19 m)
C1
C2
C3
C4
C5
C6

Figure 13

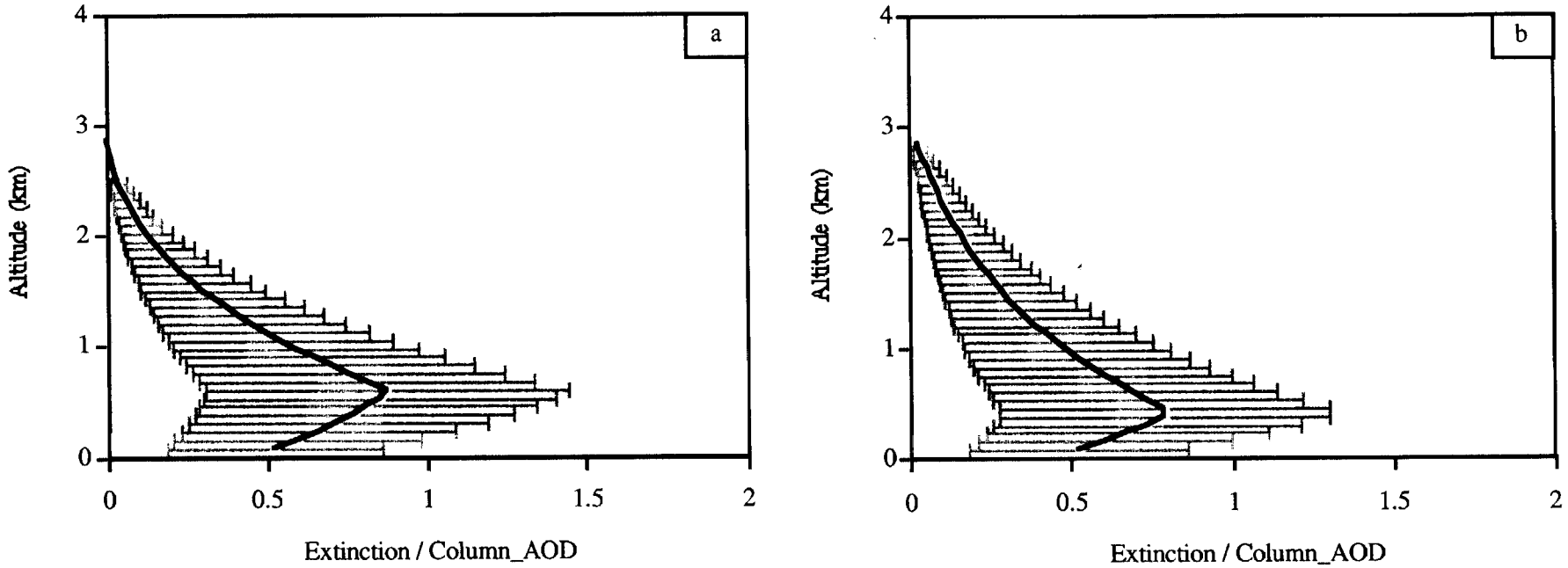

June 11, 2001

Measurements of aerosol vertical profiles and optical properties during INDOEX 1999 using micro-pulse lidars

Authors:
Ellsworth J. Welton*, Kenneth J. Voss, Patricia K. Quinn, Piotr J. Flatau, Krzysztof Markowicz, James R. Campbell, James D. Spinhirne, Howard R. Gordon, and James E. Johnson

Submission to Journal of Geophysical Research - Atmospheres

The rapid rise in population and development in the Indian sub-continent has caused a significant increase in the amount of atmospheric pollution present in the surrounding region. In particular, researchers began to notice that large pollution plumes from India were moving out across the Indian Ocean and affecting areas that would otherwise be pristine, pollution-free, environments. In order to fully understand the causes of the pollution and the environmental and climatic impacts caused by it's transport, an international team of investigators assembled a multi-year regional study called the Indian Ocean Experiment, or INDOEX. INDOEX was lead by researchers at Scripps Institution of Oceanography and the Max-Planck Institut für Chemie (including Paul Crutzen, 1995 Nobel Laureate in Chemistry). Researchers from many other institutions worldwide also took part in INDOEX, and together compiled the instrumentation and support needed for the project.

During 1999, an intensive field study took place as part of INDOEX. Scientists from the University of Miami, Scripps, and Goddard Space Flight Center worked together to deploy mobile instrumentation to measure the vertical distribution of pollution plumes and natural background aerosols (airborne particles such as sea-salt) over the Indian Ocean. The instruments are referred to as micro-pulse lidars. The lidars use pulses of eye-safe laser light to probe the vertical distribution of aerosols and clouds, in much the same way radar is used to determine an object's distance. The lidars are also capable of determining the amount of sunlight scattered and absorbed by the aerosols, and thereby help assess their impact on the region's climate. One lidar was installed onboard the NOAA ship R/V Ronald H. Brown, and acquired data as the ship sailed from the Southern to Northern Indian Ocean. The other lidar was installed near the INDOEX headquarters on an island in the Maldives Islands, situated approximately 1000 miles southwest of India.

The results of this work are described in the attached paper. The major findings from this work show that the Southern Indian ocean was almost entirely free of continental pollution, but the Northern Indian ocean, from near the equator to the Arabian Sea, contained a very polluted layer of continental aerosols to a height of about 4 km. These results were used to develop a model of the vertical distribution of aerosols over the Indian Ocean. The results are also being used to help develop algorithms to use for processing future satellite-based lidar data that will be acquired over the Indian Ocean.

* Lead Author: Dr. E. J. Welton
GESTC/UMBC, GSFC Code 912
welton@virl.gsfc.nasa.gov